Vol. 89 No. 2 pp. 369–388 ACTA GEOLOGICA SINICA (English Edition) Apr. 2015

Tectonic Evolution of the Meso-Tethys in the Western Segment of Bangonghu-Nujiang Suture Zone: Insights from Geochemistry and Geochronology of the Lagkor Tso Ophiolite

YUAN Yajuan[1,2], YIN Zhengxin[1,2], LIU Weiliang[1,2], HUANG Qiangtai[1,2], LI Jianfeng[3], LIU Hongfei[4], WAN Zhifeng[1,2], CAI Zhourong[1,2] and XIA Bin[1,2,3,*]

1 *School of Marine Sciences, Sun Yat-sen University, Guangzhou 510275, Guangdong, China*
2 *Key Laboratory of Offshore Oil Exploration and Development of Guangdong Higher Education Institutes, Guangzhou 510275, Guangdong, China*
3 *Guangzhou Institute of Geochemistry, Chinese Academy of Sciences, Guangzhou 510640, China*
4 *Xizang Geological Survey, Lhasa 850001, Tibet, China*

Abstract: The subduction of the Bangonghu-Nujiang Meso-Tethys and the collision between the Lhasa and Qiangtang blocks were important events in the growth of the Tibetan crust. However, the timing of collision initiation and closure timing, as well as nature and structure of the Bangonghu ocean basin, are still poorly constrained. The Lagkor Tso ophiolite, located in the south of Gerze County, Tibet, is one of the most completed ophiolites preserved in the southern side of the Bangonghu-Nujiang suture zone. This study discussed the tectonic evolution of the Bangonghu-Nujiang suture zone as revealed by the Lagkor Tso ophiolite investigated by field investigations, petrology, geochemistry, geochronology and tectonic analysis methods. We present new LA-ICP-MS zircon U-Pb and $^{39}Ar/^{40}Ar$ ages for the Lagkor Tso ophiolite, in addition to geochemical and platinum-group element (PGE) data presented for the Lagkor Tso ophiolite in Tibet. It is suggested that the ancient Lagkor Tso oceanic basin split in Middle Jurassic (161.2 ± 2.7 Ma – 165.4 ± 3.5 Ma), and experienced a second tectonic emplacement during the Early Cretaceous (137.90 ± 6.39 Ma). The Lagkor Tso ophiolite likely developed in an independent suture zone. The Bangonghu-Nujiang ocean subducted southwards, and the dehydration of the subducting oceanic crust materials caused partial melting of the continental mantle wedge, which formed the second-order expanding center of the obduction dish. This led to inter-arc expansion, followed by the formation of inter-arc and back-arc basins with island arc features, which are represented by ophiolites around the Shiquanhe-Lagkor Tso -Yongzhu region. The tectonic environment presently can be considered to be similar to that of the current Western Pacific, in which a large number of island arc-ocean basin systems are developed.

Key words: ophiolite, geochemistry, geochronology, inter-arc basin, Lagkor Tso, Bangonghu-Nujiang suture zone

1 Introduction

Ophiolites, representing relict fragments of ancient oceanic crust distributed across suture zones, are one of the most important boundary structures produced by ancient plate tectonics (Dietz et al., 1970; Coleman, 1977; Zhou, 1996; Zhang et al., 2003; Robertson, 2002). The tectonic emplacement of ophiolites indicates the beginning of continental collision, and thus provides constraints on the continental dynamics during initial collision and ocean-continent transition.

The Tibetan Plateau consists of multiple suture zones separating various ancient terranes (Xiao and Wang, 1984; Chang et al., 1988; Xia et al., 1989; Pan et al., 1996; Wu et al., 2013). The Yarlung Tsangpo suture zone and the Bangonghu-Nujiang suture zone represent a disappeared Neo-Tethys, which existed between the Gondwanan and Laurasian continents (Fig.1).

Since the 1970s, the Bangonghu suture zone has been studied by both domestic and foreign researchers. However, general mechanisms for the formation and

* Corresponding author. E-mail: xb698xy@qq.com

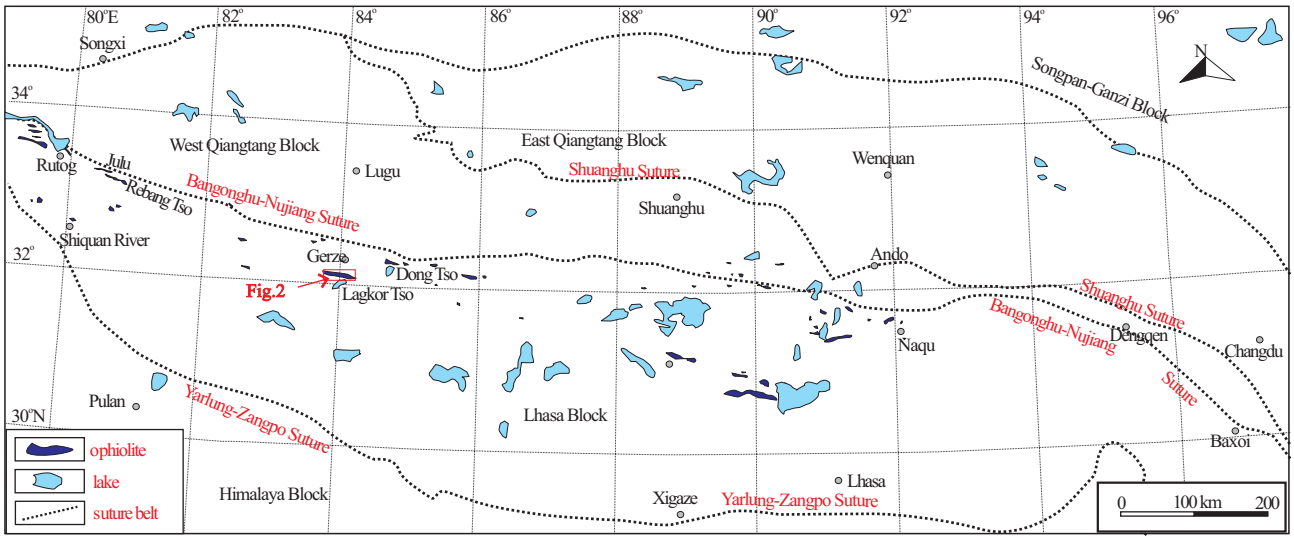

Fig.1. Sketch map of the Bangonghu–Nujiang suture showing distribution of ophiolitic fragments (modified from Zhang et al. (2012) and Zhu et al. (2013)).

evolution of this zone are still generally understood, and many important issues remain to be further discussed. For example, there is yet no consensus for the timing of collision initiation and closure of the Bangonghu ocean basin (see Zhang et al., 2012 for a review). In addition, there are different opinions about the tectonic nature and structure of the Bangonghu ocean basin, which has been suggested to be a normal ocean (Ye et al., 2004; Bao et al., 2007), or alternatively a supra-subduction-zone (SSZ) basin (Allègre et al., 1984; Girardeau et al., 1984, 1985; Pearce and Deng, 1988; Zhou et al., 1997; Kapp et al., 2003; Zhang et al., 2007a; Li et al., 2013), or a back-arc basin (Wang et al., 2008; Liu et al., 2014).

The Gerze Lagkor Tso ophiolite, located in the southern part of Gerze County, Tibet, extends NWW–SEE. It borders the Shiquanhe ophiolite in the west, the Asuo-Yongzhu-Namu Tso ophiolite in the east and extends from Jiali and Bowo to Zay in the east. It is thousands of kilometers in length from east to west and between 3 and 35 km in width from south to north, referred to as the Shiquanhe-Lagkor Tso-Asuo-Yongzhu-Namu Tso-Jiali-Bowo arc-arc collision zone, which was termed the Slainajap zone for easy reference (Pan et al., 2004, 2006).

Previous researchers have conducted many valuable investigations into the formation and evolution of the Lagkor Tso ophiolite. Each of these resulted in different genesis models, as a result of differing initial viewpoints and different data sets. In general, three broad formation mechanisms have been suggested: (1) the Lagkor Tso ophiolite is the product of southward thrust of the Tong Tso ophiolite (Girardeau et al., 1984; Tibet Bureau of Geology and Minerals Resources, 1993); (2) the Lagkor Tso ophiolite is a part of the Bangonghu-Nujiang suture (Xiao and Li, 2000; Zhang et al., 2007b); and (3) the Lagkor Tso ophiolite was formed and developed in a separate inter-arc basin, and represents the product of an arc-arc collision independent of the Bangong-Nujiang suture zone and the Yarlung Tsangpo suture zone zone (Pan et al., 1997, 2004, 2006; Li and Qu, 1993; Wang et al., 2007).

The ophiolites were thought to have been formed during the late Jurassic to early Cretaceous, based on a SHRIMP zircon U-Pb age (155.3 ± 2.6 Ma) obtained for the plagioclase granite, a whole rock K/Ar age (124 Ma) for the basalts, and a whole rock $^{39}Ar/^{40}Ar$ age (124.63 ± 0.6 Ma) for the gabbro (Tibet Bureau of Geology and Minerals Resources, 1987; Geology Investigation Institute of Sichuan Province, 2006). However, Zhang *et al.* (2007b) reported that the Lagkor Tso ancient oceanic basin began to split during the middle Jurassic (166.6 ± 2.5 Ma). Thus, there are significant discrepancies in the scientific understanding of the formation and emplacement times of the Lagkor Tso ophiolite, as well as its tectonic environment.

In this paper, new LA-ICP-MS zircon U-Pb ages and $^{40}Ar/^{39}Ar$ ages are presented for the Lagkor Tso ophiolite in Tibet, in addition to new geochemical and platinum-group element (PGE) data, in an attempt to constrain the tectonic history and structure of the Bangonghu Meso-Tethys.

2 Geological Setting

The Lagkor Tso ophiolite occurs around the Lagkor Tso 30 km south of the Gerze County, Tibet. On its southern side, a second-order tectonic unit of the Gangdise-Nyainqentanglha composite volcanomagmatic arc (also called the Zenong volcanomagmatic arc) is developed. The continental crust basement of Zenong volcanic arc was formed in a normal Late Paleozoic normal continental

shelf sedimentary environment, while the arc body, comprising mainly the Jienu Group ($J_2 - J_3$), the Zenong Group ($J_3 - K_1$) and the Jiega Group (K_1), makes up a complete multi-volcanic sedimentary cycle assemblage of andesitic basalt, andesite, rhyolite and intermediate-acid pyroclastic rocks. To the north of the ophiolite is a close neighbor of a second-ordered tectonic unit of the Anglongangri-Bange-Baishula magmatic arc, named the Bochangzangbo-Selingcuo front-arc continental shelf belt. The main body of this belt comprises the Early Cretaceous Duoni Formation and Langshan Formation shallow-sea sediments (Pan et al., 2002, 2006).

The Lagkor Tso ophiolite itself extends almost 30 km in length from east to west and spans 3–6 km in width from south to north, covering a total area of 120 km^2 (Fig. 2). To the south and north, most of the ophiolite is in fault contact with the Langshan Group (K_1), with local contact with the Zenong Group (J_3–K_1). Although the ophiolite has undergone complex tectonic movements, its sequence is basically complete, including peridotite, cumulate rocks, pillow lavas, diabase and gabbro dyke swarms, plagiogranites and radiolarian siliceous rocks units(Fig. 3).

Lherzolite (32°06′07.2″N, 83°58′05.2″E) is of weak serpentinization, false spot structure, grid structure.

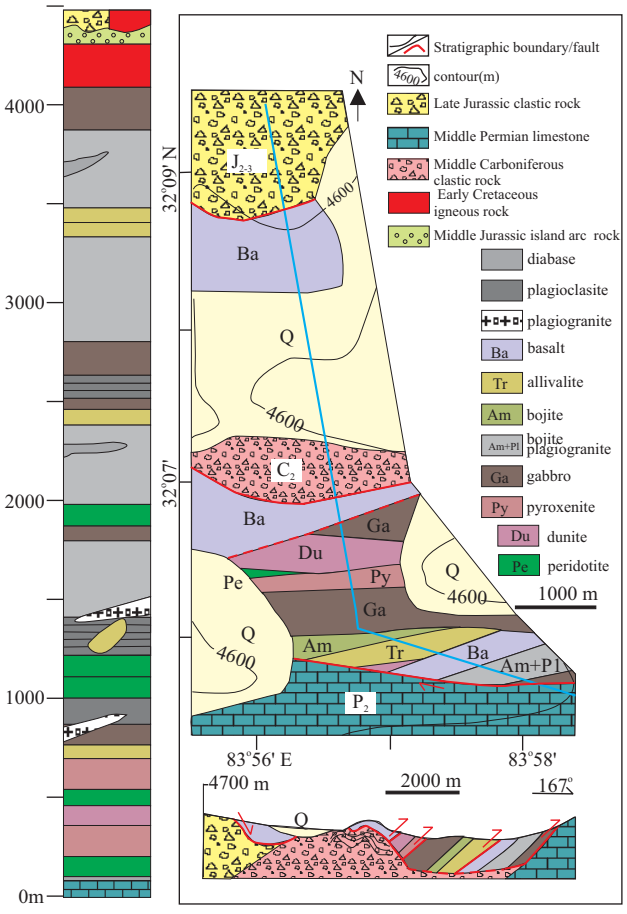

Fig.2. Simplified geologic map of Lagkor Tso ophiolite (modified from Zhang et al. (2007b)).

Residual olivine show kink bands (at center). The tremolitized clinopyroxene fragments display pseudomorph of dense exsolution lamellae. Clinopyroxene particles are recrystallized in euhedral form in balanced crystalloblastic texture (Fig. 4a).

The main mineral orthopyroxene in spinel harzburgite (32°06′07.2″N, 83°58′05.2″E) shows the mortar and broken base which are all plastically deformed. Olivine shows not only kink bands, but also kink lines (fine and dense wavy lines at center). Kink band is also shown in the orthopyroxene at the lower-middle side. Meanwhile, exsoluted materials from orthopyroxene in two phases are clearly shown (Fig. 4b).

Gabbro (32°05′27.1″N, 84°08′29.7″E) is overall dark gray in fibrous crystalloblastic texture and palimpsest-ophitic texture in massive structure. Rocks are strongly uralitized. Mineral particles are sized generally 1–3mm. Mineral compositions are mainly clinopyroxene, basic plagioclase, and hornblende (Fig. 4c). Individual rocks are subjected to strong prehnitized or uralitized.

Pillow basalts (32°04′54.2″N, 84°10′24.7″E) are grayish green, less phenocrysts. The phenocrysts, 1%-2% of total amount, are euhedral to subhedral tabular plagioclase, and all are saussuritized in pseudomorph. The textures of the matrix vary largely in each lava unit, even in different parts of pillow-like bodies. The pillow-like bodies feature aphanitic margin in intersertal texture. The central parts of pillow-like bodies and lava units show quasi-intergranular and microcrystalline textures, and composed of mainly plagioclase and pyroxene. The plagioclase, occupying 45% to 50% of total, euhedral to subhedral small lath shaped, are largely saussuritized; Pyroxenes, 45% to 50% in amount, are metasomatized with ouralite and chlorite, often in fibrous distribution (Fig. 4d). Accessory minerals are magnesioferrite and apatite. The rock has been altered into spilite.

The adcumulatic quartz diorite contains hornblende and plagioclase. A hornblende includes several plagioclase, apatite, and euhedral sulfide crystals, showing adcumulate texture. Outside the hornblende is cumulate plagioclase showing bright bands of albite (Fig. 4e).

Olivines in the Olivine diabase are iddingsitized as anhedral fragments that sandwiched between plagioclase and hornblende. Pyroxenes are amphibolized with residuals. Pyroxene-hornblende crystals are in clear poikilitic texture with feldspar grains. Ilmenite is oxidized to some degrees (Fig. 4f).

3 Analytical Techniques

3.1 Whole-rock major, trace element and PGE analyses

We collected 21 rock samples (including peridotite,

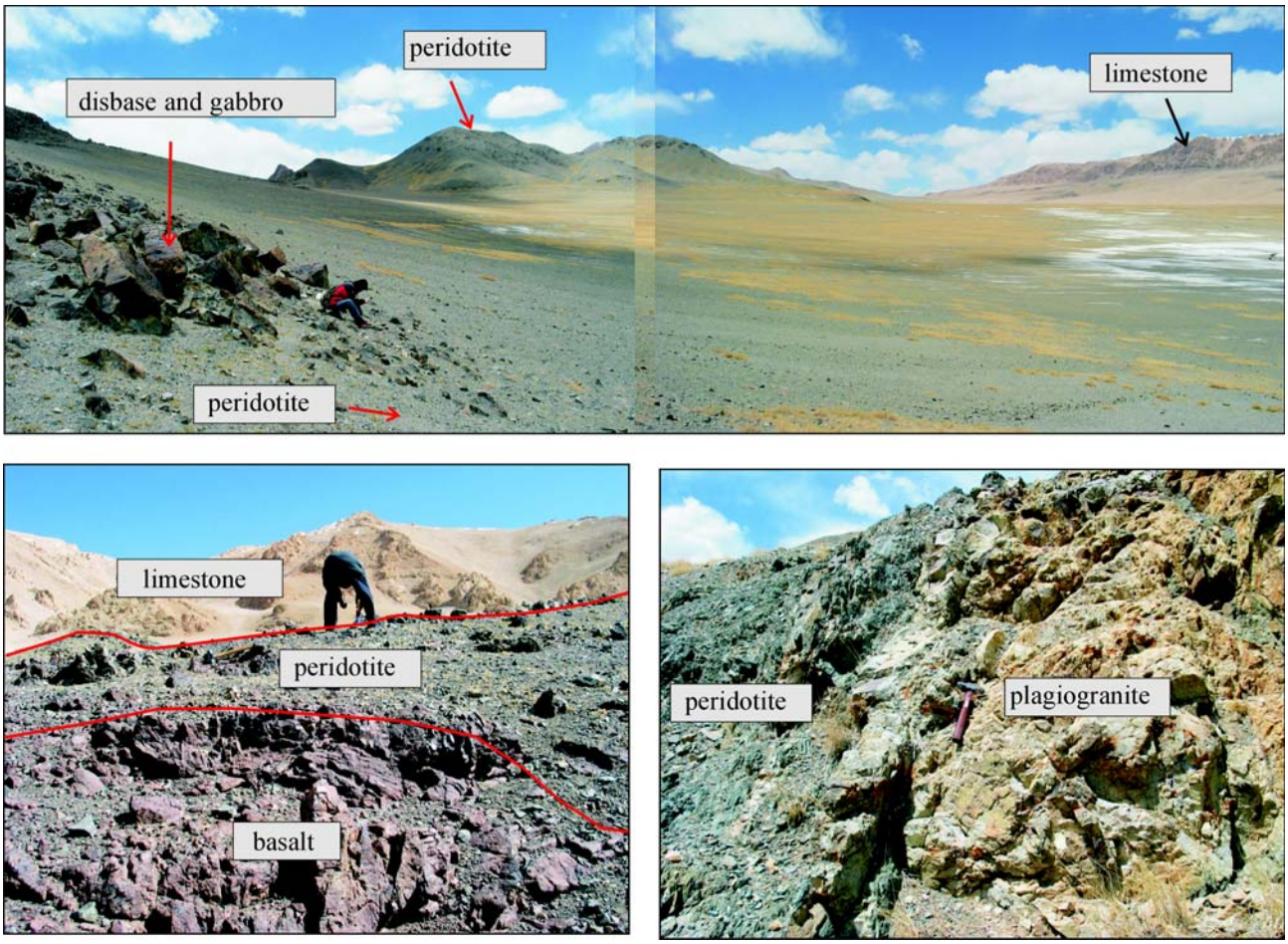

Fig.3. Field photographs showing field relations and lithologies of Lagkor Tso ophiolite.

cumulate rocks and pillowed laves) for major and trace elements (including REE and PGE) analyses(Table 1). The samples were collected so as to avoid vein fillings and alteration rinds, cleaned and then powdered to less than 200 meshes for whole-rock analyses using an agate mill. Major elements were measured by X-ray fluorescence (XRF) method at the Guangzhou Institute of Geochemistry, Chinese Academy of Sciences, Guangzhou, China, using fused glass beads (0.5 g rock powder and 2.5 g $LiBO_3$ flux) following the method of Norrish and Hutton (1969). The precision was better than ±2% (relative) for a concentration of 0.5 wt%. Trace elements were analyzed using a PE Elan 6000 ICP-MS at the Institute of Geochemistry, Chinese Academy of Sciences, Guiyang, China. Samples were dissolved using a mixed acid of HNO_3 and HF. The procedure is the same as that described in Qi *et al.* (2000). The analytical results and the uncertainties of reference materials were estimated to be better than ±5–10% (relative) for most elements. Analyses of PGE were also carried out at the Institute of Geochemistry, Chinese Academy of Sciences, Guiyang. Samples were decomposed using Na_2O_2 fusion, pre-concentrated by Te co-precipitation, and analyzed by the isotope dilution ICP-MS method (Qi et al., 2003). A Finnigan MAT ELEMENT-type high-resolution ICP-MS was used for determining PGE, except Os whose oxides are volatile, which because the formation and loss of highly volatile OsO_4 were unavoidable during this chemical preparation. Analytical results of international reference standards are certified reference materials from Canadian Standard Reference Centre. The analytical results (ppb) of international reference standards were listed in table 2.

3.2 Zircon U-Pb dating

Zircons were separated from sample B176-G+B and B137-G, concentrated using heavy liquid and isodynamic magnetic separators, and handpicked under a binocular microscope. They were mounted in epoxy resin and polished to approximately half their thickness, before examination of internal structures by backscattered electron (BSE) imaging using a scanning electron microscope (SEM) and optical microscopy in order to ensure that the zircons analyzed during this study were the least fractured, and were inclusion free. Sample

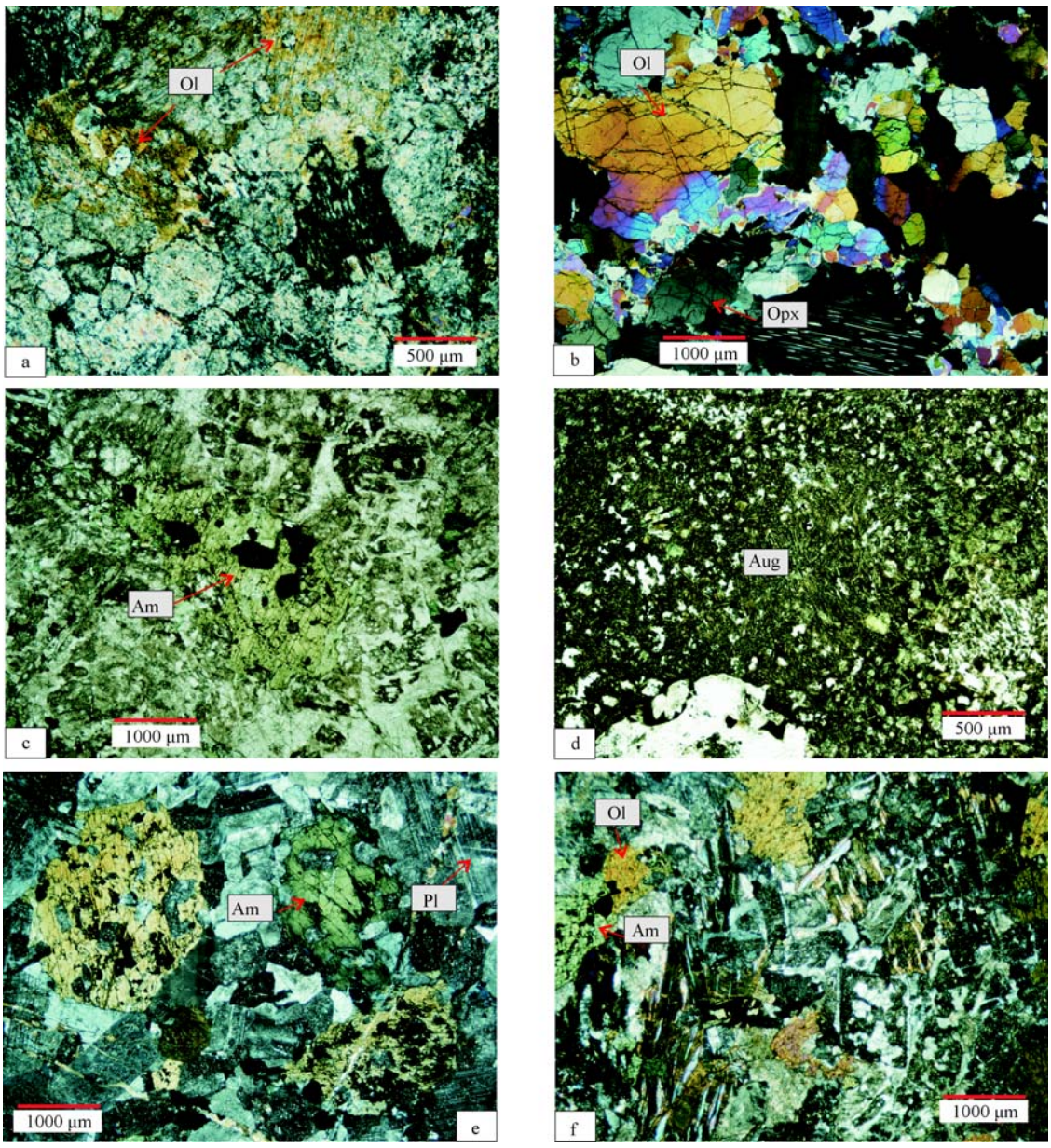

Fig. 4. Microphotos show characters of the minerals in Lagkor Tso ophiolite.

preparation was undertaken at the Guangzhou Institute of Geochemistry, Chinese Academy of Sciences.

Zircon U-Pb dating was undertaken using laser ablation inductively coupled plasma mass spectrometry (LA-ICP-MS) at the State Key Laboratory of Isotope Geochemistry, Guangzhou Institute of Geochemistry. Execution of sample target, operation and data processing procedures have been described. Internal structure was examined using cathodoluminescence (CL) images prior to U-Pb isotopic analyses. The LA-ICP-MS system used consisted of an Agilent 7500a ICP-MS coupled with a Resonetics RESOlution M-50 ArF Excimer laser source (λ = 193 nm), using a laser energy of 80 mJ, a repetition rate of 10 Hz, a spot diameter of 31 μm, and a 40 s ablation time. Helium was used as a carrier gas to carry ablated aerosols to the ICP source, and NIST610 and TEM ($^{206}Pb/^{238}U$=416.8 Ma) were used as external calibration standards, with ^{29}Si used as an internal standard.Common Pb was corrected by using observed 204Pb. Uncertainties of data points listed in Table 2 are given at ±1σ.The ages quoted in the text are $^{206}Pb/^{238}U$ (the older age is $^{207}Pb/^{206}Pb$ ages) ages, which are the weighted mean at the 95% confidence level. The software of ICP-MS Datacal 7.4 and attached IsoplotI/Ex_ver3 were used for data processing (Ludwing, 2003; Liu et al., 2008, 2010).

3.3 Amphibole $^{40}Ar/^{39}Ar$ geochronology

One sample (XLG-10) of amphibole for $^{40}Ar/^{39}Ar$ dating was collected from the plagioclase amphibolites in the thermal contact metamorphic zone during the same

Table 1 Major, trace elements and PGE abundances of the Lagkor Tso ophiolite units

Sample	Cumulate rocks										
	B137–Z	B138–Z	B142–G	B145–Z	B171–G	B175–Z–G	B180–Z	B183–G–Z	B191–Z–1	B192–Z–2	B191–Z–3
Major elements (wt%)											
SiO_2	56.45	53.12	62.6	60.09	66.75	64.99	56.3	69.98	62.52	67.33	64.66
TiO_2	0.9	0.88	0.55	0.1	0.44	0.43	1.51	0.41	0.22	0.19	0.13
Al_2O_3	17.77	18.93	14.55	11.44	15.6	15.29	14.3	13.53	10.2	10.42	12.35
Fe_2O_3	8.44	8.26	6.65	7.63	5.24	5.7	12.75	4.36	6.79	6.84	5.63
MnO	0.17	0.15	0.13	0.16	0.16	0.15	0.23	0.13	0.13	0.09	0.09
MgO	2.21	3.25	3.21	8.23	1.46	1.89	5.46	1.04	4.27	2.82	3.07
CaO	6.77	6.73	4.75	1.79	3.1	2.86	4.61	3.32	7.34	3.5	3.28
Na_2O	3.66	3.58	4.22	2.77	4.69	5.77	4.09	4.6	4.14	4.08	5.26
K_2O	0.48	0.68	0.39	0.11	0.42	0.19	0.11	0.69	0.09	0.06	0.35
P_2O_5	0.211	0.172	0.09	0.027	0.091	0.132	0.154	0.078	0.108	0.03	0.027
LOI	1.37	2.78	2.29	6.15	1.68	1.14	0.64	1.19	2.85	3.34	3.22
Total	98.46	98.57	99.47	98.55	99.67	98.57	100.2	99.36	98.72	98.74	98.11
Trace elements (ppm)											
Sc	29	20	22	31	10	7	31	13	28	24	23
Ti	0.41	0.4	0.31	0.07	0.25	0.26	0.77	0.23	0.11	0.11	0.09
V	130	178	130	167	37	40	379	45	200	199	201
Cr	150	140	170	440	160	170	80	200	330	230	230
Mn	1280	1120	1000	1200	1250	1150	1630	1010	1010	708	703
Co	18	20.4	15.1	27.7	7.8	8.9	34.8	7.7	28.1	26.1	20.8
Ni	22	17	16	71	16	13	29	19	71	35	49
Zn	53	54	49	71	49	66	76	36	37	46	32
Ga	17.2	16	14.4	8.9	16.4	16.2	15.1	13.8	10.5	9.3	8.2
Rb	8.8	16.3	6	2.2	8	3.4	2	10	1.3	1.1	4.1
Sr	175	191	149.5	56.4	162	120	105.5	82	176.5	146.5	184
Y	26.8	18.9	26.1	3.3	16.6	18.7	20.7	34.9	7.8	5.3	3.9
Zr	58	38	70	19	101	113	91	108	33	30	17
Nb	2.2	1.7	1.8	1.3	2.9	3.9	6.7	2.7	0.7	0.7	0.4
Cs	0.78	0.86	0.42	2.01	0.4	0.17	0.37	0.16	0.13	0.35	0.25
Ba	57.7	84.9	73.8	34.1	71.8	36	25.2	76.7	27.4	28.6	93.6
Hf	1.7	1.2	2.3	0.6	2.9	3.1	2.5	3.5	1	0.9	0.5
Ta	0.1	0.1	0.1	0.1	0.2	0.3	0.5	0.2	0.08	0.08	0.08
Th	0.84	0.99	1.58	0.59	4.79	5.4	0.9	2.74	0.51	0.32	0.23
U	0.19	0.2	0.39	0.21	0.51	0.71	0.26	0.68	0.16	0.15	0.2
La	4.3	4.6	5.8	1.8	12.4	13.5	7.4	9.1	3.4	1.9	1.1
Ce	10.8	10.6	13.7	3.6	25.2	29.4	16.1	20.8	5.2	2.7	1.7
Pr	1.69	1.51	1.9	0.41	2.82	3.55	2.21	2.81	0.61	0.33	0.23
Nd	9.2	7.4	9.3	1.6	10.9	13.8	10.4	13.3	2.8	1.5	1.1
Sm	3.05	2.32	2.76	0.37	2.42	2.99	2.86	3.78	0.73	0.44	0.36
Eu	1.15	0.84	0.91	0.09	0.8	0.88	0.95	1.05	0.28	0.17	0.13
Tb	0.82	0.56	0.72	0.09	0.48	0.55	0.61	0.94	0.18	0.12	0.1
Gd	3.84	2.76	3.38	0.41	2.62	2.93	3.08	4.57	0.94	0.59	0.48
Dy	5.2	3.47	4.73	0.56	2.9	3.19	3.77	6.12	1.2	0.88	0.74
Ho	1.13	0.76	1.03	0.13	0.62	0.71	0.82	1.37	0.27	0.2	0.16
Er	3.19	2.19	3.14	0.41	1.93	2.17	2.35	4.16	0.82	0.6	0.52

Table 1 Continued

Sample	Cumulate rocks										
	B137–Z	B138–Z	B142–G	B145–Z	B171–G	B175–Z–G	B180–Z	B183–G–Z	B191–Z–1	B192–Z–2	B191–Z–3
Tm	0.43	0.32	0.47	0.08	0.3	0.34	0.35	0.63	0.12	0.1	0.08
Yb	2.66	2.08	2.95	0.56	1.99	2.26	2.33	4.12	0.81	0.7	0.54
Lu	0.4	0.32	0.48	0.11	0.33	0.37	0.36	0.66	0.13	0.11	0.09
ΣREE	47.86	39.73	51.27	10.22	65.71	76.64	53.59	73.41	17.49	10.34	7.33
δEu	0.34	0.33	0.30	0.23	0.32	0.30	0.32	0.25	0.34	0.33	0.31
$(La/Sm)_N$	0.91	1.28	1.36	3.14	3.31	2.91	1.67	1.55	3.01	2.79	1.97
$(La/Yb)_N$	1.16	1.59	1.41	2.31	4.47	4.28	2.28	1.58	3.01	1.95	1.46
Sample	Pillow basalts							Mantle peridotite			
	B176–G–Z	11LGC–10	11LGC–21	11LGC–22		B132–Z	B134–Z	B136–Z	B190–Z	B134–1	B136
Major elements (wt%)											
SiO_2	48.43	52.71	52.92	52.67		39.46	36.46	36.13	40	41.04	41.42
TiO_2	0.66	0.83	0.21	0.23		0.01	0.02	0.09	0.01	0.05	0.11
Al_2O_3	18.39	17.28	16.65	16.54		0.16	3.64	2.1	0.23	4.10	3.16
Fe_2O_3	10.88	6.56	6.33	6.73		8.44	9.39	11.25	5.05	12.23	12.69
MnO	0.21	0.07	0.09	0.08		0.08	0.15	0.16	0.12	0.17	0.18
MgO	5.47	7.67	6.41	5.58		37.6	35.22	35.45	40.37	41.01	41.06
CaO	9.46	5.74	5.13	5.75		0.01	0.35	0.13	0.06	0.46	0.28
Na_2O	2.6	4.58	6.58	5.06		0.01	0.01	0.01	0.01	0.02	0.01
K_2O	1.05	0.37	0.26	0.18		0.01	0.01	0.01	0.01	0.01	0.01
P_2O_5	0.03	0.13	0.03	0.02		0.01	0.01	0.01	0.01	0.01	0.01
LOI	2.79	3.41	5.06	6.42		12.3	12.45	12.25	13.7	12.07	15.27
Total	99.97	99.35	99.67	99.26		98.45	98.4	98.27	99.91	99.11	98.94
Trace elements (ppm)											
Sc	27	24.9	34.3	34.9		4	8	9	3	10	8
Ti	3956	4975	1259	1379		59.94	119.88	539.46	59.94	493.98	215.33
Cr	120	78.8	88.7	104		2470	4610	4810	2000	3901	3165
Mn	1560	627	806	716		576	1220	1260	885	1099	1032
Co	32.1	25.4	23.3	24		112	121	132	108	111	102
Ni	17	33.7	238	145		2380	1615	1855	2010	1551	1313
Zn	59	58.2	62.4	55.6		44	66	68	27	75	65
Ga	16.7	15.5	11.2	10		0.5	3.1	3	1.2	3.6	3.3
Rb	37.2	11.2	0.753	3.46		0.2	0.2	0.3	0.5	1.3	1.3
Sr	201	250	133	86.4		1.7	3.1	2.9	1.3	3.2	2.9
Y	7.5	18.9	5.63	4.98		0.7	0.5	0.9	1.8	1.3	0.7
Zr	28	107	24.2	23.7		18	5	3	35	5	5
Nb	0.6	3.47	0.63	0.49		0.3	0.16	0.16	0.16	2.33	2.32
Cs	1.52	2.21	0.12	0.344		0.05	0.008	0.008	0.62	0.08	0.07
Ba	278	51.9	22.5	116		1.2	2.1	2.9	0.6	2.1	2.8
Hf	0.9	2.83	0.68	0.64		0.4	0.16	0.16	0.8	0.25	0.23
Ta	0.1	0.34	0.10	0.05		0.08	0.08	0.08	0.08	0.09	0.08
Th	1.69	3.32	0.31	0.25		0.09	0.04	0.04	0.07	0.05	0.05
U	0.31	0.80	0.15	0.09		0.05	0.04	0.04	0.04	0.09	0.11
La	4.2	11	2.03	1.15		0.7	0.4	0.4	0.6	0.7	0.6
Ce	7.6	21.1	3.76	2.37		1.3	0.4	0.4	0.5	0.4	0.4

Table 1 Continued

Sample	Pillow basalts				Mantle peridotite					
	B176–G–Z	11LGC–10	11LGC–21	11LGC–22	B132–Z	B134–Z	B136–Z	B190–Z	B134–1	B136
Pr	0.86	2.71	0.41	0.28	0.16	0.04	0.05	0.08	0.07	0.05
Nd	3.5	11.8	1.71	1.26	0.6	0.2	0.2	0.4	0.83	0.70
Sm	0.87	2.75	0.40	0.37	0.14	0.05	0.09	0.16	0.15	0.17
Eu	0.33	0.87	0.17	0.12	0.14	0.05	0.06	0.06	0.14	0.12
Tb	0.22	0.54	0.12	0.09	0.03	0.01	0.02	0.04	0.04	0.01
Gd	1.04	3.22	0.55	0.5	0.15	0.06	0.12	0.18	0.09	0.07
Dy	1.32	3.44	0.81	0.64	0.15	0.08	0.16	0.28	0.42	0.33
Ho	0.29	0.71	0.18	0.15	0.03	0.02	0.04	0.06	0.13	0.10
Er	0.88	2.02	0.58	0.49	0.07	0.06	0.11	0.19	0.16	0.09
Tm	0.13	0.34	0.1	0.08	0.01	0.01	0.02	0.03	0.03	0.02
Yb	0.88	1.94	0.58	0.59	0.06	0.07	0.14	0.2	0.20	0.12
Lu	0.15	0.31	0.10	0.09	0.01	0.01	0.02	0.03	0.04	0.02
ΣREE	22.27	62.75	11.50	8.17	3.55	1.46	1.83	2.81	3.40	2.82
δEu	0.35	0.29	0.36	0.28	0.97	0.91	0.58	0.35	1.26	1.10
$(La/Sm)_N$	3.12	2.59	3.29	2.03	3.23	5.16	2.87	2.42	3.01	2.28
$(La/Yb)_N$	3.42	4.07	2.52	1.40	8.37	4.10	2.05	2.15	2.56	3.46
PGE(ppb)	B190–Z	B134–1	B136	PGE(ppb)	B190–Z	B134–1	B136	PGE(ppb)	B190–Z	B134–1	B136
Ir	0.121	0.182	0.060	Rh	0.175	0.334	0.203	Pd	1.906	1.129	1.241
Ru	1.625	1.869	0.424	Pt	0.830	0.585	2.508	ΣPGE	4.656	4.099	4.436

period with the tectonic emplacement. The amphibole was purified and crushed, repeatedly sieved to uniform mineral grains of 0.5–2 mm, washed in an ultrasonic bath of distilled water for 1 h and then dried. And it was observed under a binocular microscope. The argon isotopes were analyzed on a GV Instruments 5400® mass spectrometer with a secondary electron multiplier (Balzers SEV217) in pulse 183 counting mode and a coherent CO_2 of 50–W laser at the State Key Laboratory of Isotope Geochemistry, Guangzhou Institute of Geochemistry, Chinese Academy of Sciences. The experimental methods and procedures have been described previously (Qiu and Jiang 2007; Qiu et al., 2010). The samples and a monitor standard ZBH-25 biotite with an assumed age of 132.5 Ma (Qiu 1996; Wang 1983) were irradiated at the 49–2 reactor in Beijing for 51h25min. The correction factors for interfering argon isotopes derived from Ca and K are as follows: $(^{39}Ar/^{37}Ar)Ca = 8.984 \times 10^{-4}$, $(^{36}Ar/^{37}Ar)Ca = 2.673 \times 10^{-4}$ and $(^{40}Ar/^{39}Ar)K = 5.97 \times 10^{-3}$. The extraction and purification lines were baked out for 20h at 150°C with heating tape, and the sample chamber was baked out with a furnace. The static blank of ^{40}Ar after 5 min was approximately 2 mV.

To correct for system blanks, the experiments began and ended with cold blank analyses, and cold blanks were also measured after every four-step sample analyses. The released gas was purified for 5 to 8 min by two Zr/Al getter pumps operated at room temperature or approximately ca. 400 °C. The purified gas was then analyzed.

4 Results

4.1 Pillow basalts

After subtraction of the Loss of Ignition (LOI) values and normalization, the pillow basalts were found to have lower TiO_2 (0.21–0.83 wt%) contents than N-MORB (1.56 wt%) (Melson et al., 1976), with an average of 0.48 wt%, which is much closer to that of oceanic island basalts (OIB, 0.58–0.85 wt%) (Pearce, 1983). In order to detect alteration, a Nb/Y versus Zr/TiO_2 discrimination diagram (Cox et al., 1979) was constructed (Fig. 5). In this, all the samples are plotted in the basalt region, is the same as those basalt samples analyzed by Wang et al. (2007).

All the pillow basalts analyzed have low total REE abundance ranging from 8.17 to 62.75 ppm, with an average of 26.20 ppm, which is 0.67 and 0.13 times that of N-MORB (39.11 ppm) and OIB (198.96 ppm), respectively (Sun and McDonough, 1989) respectively. Additionally, the pillow basalts are enriched in light REEs (LREEs) (Fig.6a), which is more consistent with the E-MORB than the N-MORB. The averages of the La/Sm and La/Yb ratios for the basalts are 2.75 and 2.85, respectively,

Table 2 Analytical results (ppb) of international reference standards

sample	UMT–1		WPR–1		TDB–1	
	Reference	Measured	Reference	Measured	Reference	Measured
Ir	8.8	8.05	13.5	12.6	4.7±1.1	5.11
Ru	10.9	10.4	22	21.5	2.5±0.2	2.21
Rh	9.5	8.94	13.4	12.80	4.3±0.8	4.73
Pt	128	133	285	305	58±5	55.3
Pd	106	105	235	225	60±9	68.3

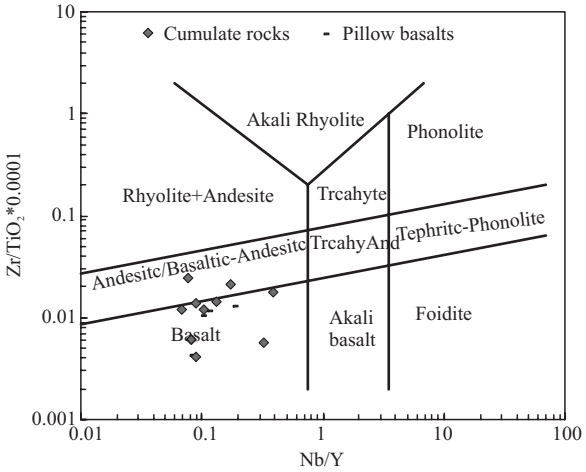

Fig. 5. Classification diagram of Zr/TiO_2 versus Nb/Y for the pillow basalts in the Lagkor Tso region.

which are closer to the E-MORB values (1.56 and 1.90, respectively) than the N-MORB values (0.61 and 0.58, respectively). In Fig.6, the pillow basalts show distribution slopes that are comparable with those from the basalts presented by Wang *et al.* (2007).

The fingerprint elements and ratios of the pillow basalts show ranges of Ta = 0.053–0.1ppm, Nb = 0.488–3.47ppm, Nb/La = 0.14–0.4, Hf/Ta = 6.9–12.1, La/Ta = 20.7–42 and Ti/Y = 23.58–276.83 (except B176-G-Z), which are apparently similar to N-MORB and OIB values and different from the WPB, T-MORB and E-MORB values (Condie et al., 1989). In the primitive mantle normalized spider diagram (Fig. 6a), the pillow lavas have similar curves to those presented by Wang *et al.* (2007), which are enriched in Large Ion Lithophile Elements (LILE) and depleted in High Field Strength Elements (HFSE), clearly displaying compositional characteristics of island-arc volcanic rocks.

4.2 Cumulate rocks

The cumulate rocks are relatively fresh, with LOI values from 0.64 wt% to 6.15 wt%. After LOI subtraction and normalization, the rocks have a SiO_2 content of 53.12–69.98 wt%, Al_2O_3 content of 10.2–18.93wt%, and TiO_2 content of 0.1–0.9 wt%. The total alkali contents range from 2.88 wt% to 5.96 wt%, with an average of 4.58wt%. With the exception of sample B145-Z, which has a high MgO content (8.23 wt%) due to its high accessory mineral (such aspyroxene) composition, the other samples have high total iron contents, from 4.62 wt% to 13.5 wt%, and low MgO contents ranging from 2.05 wt% to 2.88wt%. The Mg numbers of the rocks range from 32.09 to 68.12, indicating a derived magma. In the Nb/Y-Zr/TiO_2 discrimination diagram after Cox *et al*. (1979) (Fig. 5), all samples are plotted in boundary region between basalt and andesite, apparently similar to the pillow basalts.

The total REE abundances of the cumulate rocks range between 7.33 and 76.64 ppm, with an average of 41.24 ppm, which is 1.05 and 0.21 times that of N-MORB and OIB, respectively. It can be seen in the REE distribution patterns (Fig. 6b) that the samples are enriched in LREEs, with a $(La/Yb)_N$ of 2.32 and no europium (Eu) anomaly; these are similar to the E-MORB values. On the basis of their REE contents, the cumulate rocks can be divided into two groups, indicating magmatic differentiation.

In the primitive mantle normalized spider diagram (Fig. 6b), the samples display similar curves, representing enrichments of LILE and LREE, and deficits of HFSE. The HFSEs in particular show relative depletions compared to the LILEs, with $(Th/Ta)_N$ and $(Th/Nb)_N$ ratios of 4.85 and 6.28 respectively; this is the characteristic of volcanic rocks affected by subduction (Pearce, 1982; Sun and Mc Donaugh, 1989; Zhang and Zhou, 2001; Lai et al., 2003).

Systematic geological and geochemical studies indicate that the cumulate rocks are characterized by high Al_2O_3 and $Na_2O>K_2O$. These rocks are enriched in LILE and LREE, but have a deficit of HFSE.

4.3 Mantle peridotite

The LOI values of the mantle peridotite range from 12.07 to 15.27%. After LOI subtraction and normalization, the rocks have a SiO_2 content of 36.13–41.42 wt%, Al_2O_3 content of 0.16–4.10 wt%, MgO content of 35.22–41.06 wt%, and TiO_2 content of 0.01–0.11 wt%, respectively. The contents of MgO in a typical harzburgite is known to be 39.6 – 48.4% (Pearce et al., 1984), therefore it is likely that metamorphic metasomatism caused the low MgO content in some of our samples. The Mg# varies from 0.88 to 0.95, showing the sample may represent the residue of partial melting of the primitive mantle. The change in Mg# may be due to a reaction between the melt and residual mantle peridotite, or to differential degrees of melting.

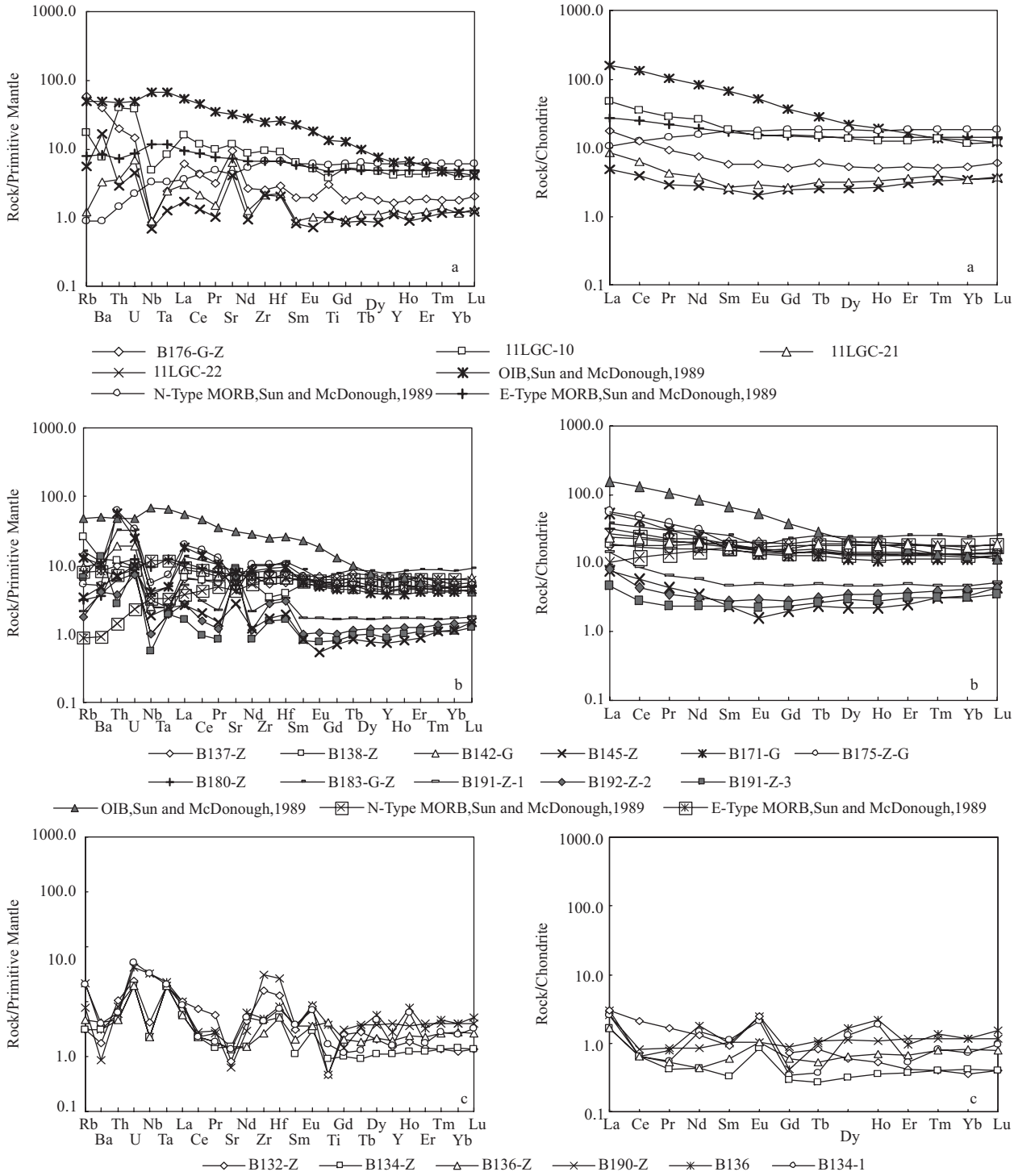

Fig. 6. Trace element spider diagram (left) and rare earth distribution pattern (right) for the volcanic rocks in the Lagkor Tso region.

The REE distribution patterns of the samples are lower than those of N-MORB, suggesting that they are characterized by depleted mantle, and the parallel curves (Fig. 6c) reflect comagmatic properties. The total REE abundances of the peridotite range between 1.46 and 3.55 ppm, with an average of 2.64 ppm; this is 0.80 and 0.07 times the values of Chondrite and N-MORB, respectively. Additionally, the REE distribution patterns (Fig. 6c) show that the samples are enriched in the LREEs, with an average $(La/Yb)_N$ of 3.78 and a positive europium (Eu) anomaly. Thus, these peridotite samples are plotted as "U" type, which show that the mantle underwent partial melting followed by metasomatism.

The total PGE concentration in the mantle peridotite of

the Lagkor Tso ophiolite is 4.099–4.656 ppb, which is 0.21–0.23 times that of the primitive mantle (20.2 ppb) and much lower than most ophiolite peridotites (Gueddari et al., 1996; Prichard et al., 1990; Oshin et al., 1982; Melcher et al., 1999; Lorand et al., 1993). The average $(Pd/Ir)_N$ and $(Pd/Ru)_N$ values of the samples are 11.64 and 1.13, respectively, which are 1.4 and 1.45 times that of a primitive mantle peridotite. The $(Pd/Ir)_N$ values of the mantle peridotite are larger than unity, reflected by positive slope of the pattern curves. The Pt/Pt* (Pt/Pt*=Pt_N/SQRT(Rh_N/Pd_N) (Hamlyn et al., 1985) values vary from 0.07 to 0.26, which represents a negative anomaly. In the primitive mantle and chondrite-normalized PGE patterns (Fig.7), the sample distribution curves are relatively similar, both falling within the Pt and Ir depleted and Ru and Rh enriched regions.

The CaO contents of the three mantle peridotite samples from the Lagkor Tso ophiolite that were tested for PGE were found to be 0.46%, 0.28% and 0.16%, while their Al_2O_3 contents were 4.1%, 3.16% and 3.29%, respectively. These values indicate a strongly depleted residual mantle left behind following a higher degree of partial melting.

The analytical results for the platinum group element (PGE) concentrations in mantle peridotites show that their total PGE contents are lower than those in most mantle peridotites worldwide. This is probably due to the extraction of sulfides from basic magmas, resulting from relatively high partial melting of the early mantle. Pt-Pd differentiation indicates that the concentrations of these two elements are likely controlled by the alloy phase and the sulfide phase, respectively. Pt was strongly incorporated into the alloy phase, while the sulfides that separated from melts were enriched in Pd. The mantle partial melting of the mantle led to the miltogenesis and separation of Pt and Pd in the crustal rocks, leading to the widespread depletion of Pt.

4.4 U-Pb zircon ages

Two samples from Lagkor Tso were selected for zircon U-Pb isotope dating (Table 3). These samples are olivine diabase (B176-G+B) and quartz diorite (B137-G) .

The zircon grains from sample B176-G+B are mostly euhedral, transparent, colorless and up to ca. 200 μm long. The grains display oscillatory zoning with no relict core and narrow zone under CL images (Fig. 8a). Their Th/U

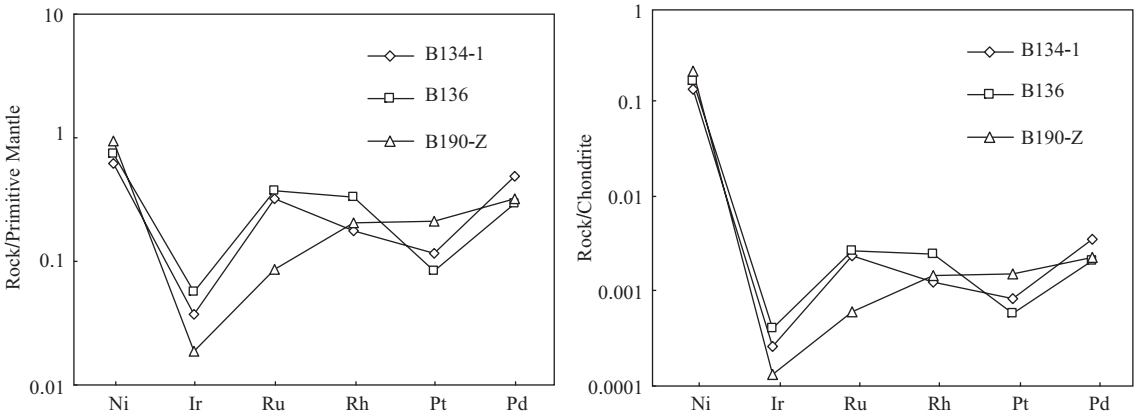

Fig. 7. Primitive mantle– normalized (left) and chondrite–normalized (right) PGE patterns for the mantle peridotite in the Lagkor Tso region.

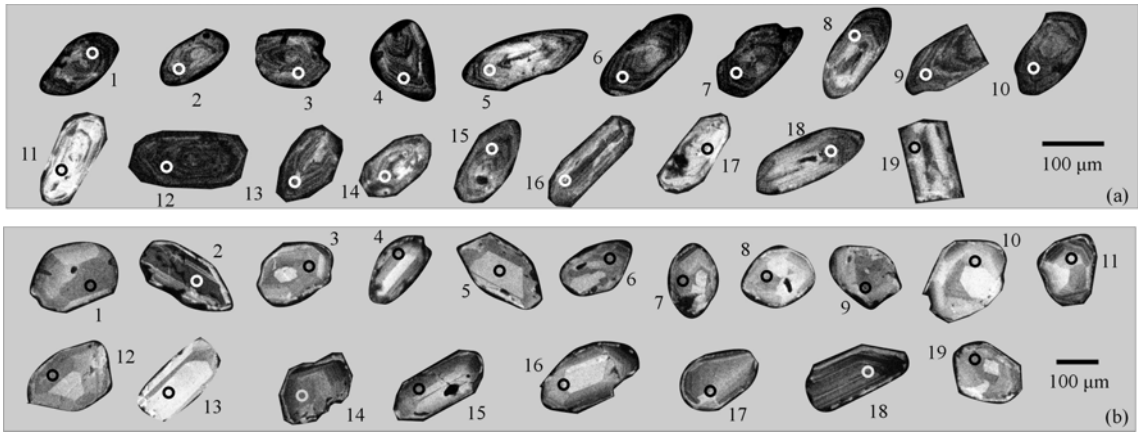

Fig. 8. Cathodoluminescence (CL) images of zircons from the Lagkor Tso olivine diabase sample B176–G+B (a) and quartz diorite sample B137–G (b). The circles represent the sites for the analysis by LA–ICP–MS.

Table 3 LA–ICP–MS zircon U–Pb isotopic data for the Lagkor Tso ophiolites in the western Bangong–Nujiang suture zone.

spot	Element (ppm)			Th/U	Isotope ratio						Apparent age(Ma)			
	Pb	Th	U		$^{207}Pb/^{206}Pb$	±1σ	$^{207}Pb/^{235}U$	±1σ	$^{206}Pb/^{238}U$	±1σ	$^{207}Pb/^{235}U$	±1σ	$^{206}Pb/^{238}U$	±1σ
Quartz diorite (B137–G)														
B137–G–1	2.9	47	94	0.50	0.05297	0.00892	0.18504	0.02840	0.02513	0.00082	172.4	24.3	159.9	5.2
B137–G–2	16.6	398	530	0.75	0.04652	0.00463	0.16933	0.01384	0.02447	0.00041	158.8	12.0	155.9	2.6
B137–G–3	3.0	33	106	0.31	0.04423	0.00759	0.16436	0.02361	0.02445	0.00071	154.5	20.6	155.7	4.5
B137–G–4	3.0	46	100	0.46	0.04913	0.01096	0.16630	0.02657	0.02456	0.00090	156.2	23.1	156.9	5.7
B137–G–5	4.9	71	160	0.44	0.04975	0.01066	0.20388	0.02811	0.02590	0.00074	188.4	23.7	164.9	4.7
B137–G–6	2.5	39	80	0.49	0.00583	0.05338	0.20304	0.04336	0.02541	0.00113	187.7	36.6	161.8	7.1
B137–G–7	2.7	28	94	0.30	0.06062	0.01048	0.22431	0.03290	0.02505	0.00085	205.5	27.3	159.5	5.3
B137–G–8	2.6	31	84	0.37	0.05287	0.00951	0.19327	0.03255	0.02637	0.00081	179.4	27.7	167.8	5.1
B137–G–9	2.6	24	96	0.25	0.07416	0.01075	0.25604	0.03472	0.02491	0.00089	231.5	28.1	158.6	5.6
B137–G–10	8.1	168	276	0.61	0.05294	0.00421	0.17706	0.01360	0.02433	0.00050	165.5	11.7	154.9	3.2
B137–G–11	3.3	51	109	0.47	0.06737	0.01090	0.21383	0.02696	0.02545	0.00081	196.8	22.6	162.0	5.1
B137–G–12	12.4	271	402	0.67	0.04952	0.00361	0.17192	0.01257	0.02524	0.00046	161.1	10.9	160.7	2.9
B137–G–13	1.9	31	63	0.49	0.08006	0.05420	0.71119	0.53586	0.03100	0.00465	545.5	329.0	196.8	29.1
B137–G–14	23.9	599	727	0.82	0.05182	0.00311	0.18819	0.01088	0.02648	0.00054	175.1	9.3	168.5	3.4
B137–G–15	6.5	75	215	0.35	0.05901	0.00531	0.21187	0.01840	0.02661	0.00062	195.1	15.4	169.3	3.9
B137–G–16	2.6	40	81	0.49	0.04784	0.01021	0.17027	0.03171	0.02696	0.00094	159.7	27.5	171.5	5.9
B137–G–17	8.7	137	296	0.46	0.04607	0.00429	0.15983	0.01371	0.02569	0.00050	150.6	12.0	163.5	3.2
B137–G–18	12.6	196	393	0.50	0.05730	0.00470	0.22506	0.01852	0.02906	0.00088	206.1	15.4	184.6	5.5
B137–G–19	3.4	39	119	0.33	0.05513	0.00703	0.17952	0.02245	0.02500	0.00085	167.7	19.3	159.2	5.4
olivine diabase (B176–G+B)														
B176–G+B–1	17.9	418	580	0.72	0.17873	0.01534	0.02529	0.00052	0.00772	0.00035	167.0	13.2	161.0	3.3
B176–G+B–2	7.6	147	254	0.58	0.16686	0.01884	0.02534	0.00065	0.00716	0.00041	156.7	16.4	161.3	4.1
B176–G+B–3	5.8	79	199	0.40	0.19914	0.02078	0.02603	0.00084	0.00714	0.00051	184.4	17.6	165.6	5.3
B176–G+B–3	20.5	471	636	0.74	0.16323	0.01273	0.02574	0.00048	0.00765	0.00032	153.5	11.1	163.8	3.0
B176–G+B–5	21.2	446	637	0.70	0.17416	0.01414	0.02737	0.00061	0.00743	0.00037	163.0	12.2	174.1	3.8
B176–G+B–6	13.3	322	432	0.75	0.14138	0.01237	0.02392	0.00055	0.00723	0.00033	134.3	11.0	152.4	3.5
B176–G+B–7	14.9	389	449	0.87	0.15489	0.01233	0.02503	0.00057	0.00810	0.00037	146.2	10.8	159.3	3.6
B176–G+B–8	19.6	385	571	0.68	0.16550	0.01342	0.02772	0.00074	0.00905	0.00046	155.5	11.7	176.3	4.6
B176–G+B–9	20.5	417	574	0.73	0.20399	0.01722	0.02800	0.00065	0.00912	0.00039	188.5	14.5	178.0	4.1
B176–G+B–10	16.6	350	534	0.66	0.17319	0.01739	0.02507	0.00056	0.00831	0.00037	162.2	15.1	159.6	3.5
B176–G+B–11	15.5	314	867	0.36	0.11111	0.00783	0.01612	0.00033	0.00545	0.00033	107.0	7.2	103.1	2.1
B176–G+B–12	17.6	383	522	0.73	0.18542	0.01392	0.02683	0.00051	0.00880	0.00041	172.7	11.9	170.7	3.2
B176–G+B–13	6.5	100	201	0.50	0.20791	0.02092	0.02773	0.00069	0.00868	0.00053	191.8	17.6	176.3	4.3
B176–G+B–14	10.5	181	337	0.54	0.18352	0.01282	0.02618	0.00050	0.00886	0.00044	171.1	11.0	166.6	3.1
B176–G+B–15	12.4	284	405	0.70	0.17254	0.01408	0.02497	0.00051	0.00747	0.00035	161.6	12.2	159.0	3.2
B176–G+B–16	15.5	332	836	0.40	0.10720	0.00730	0.01625	0.00035	0.00579	0.00027	103.4	6.7	103.9	2.2
B176–G+B–17	17.7	378	548	0.69	0.16893	0.01158	0.02563	0.00041	0.00855	0.00039	158.5	10.1	163.1	2.6
B176–G+B–18	19.5	486	583	0.83	0.17281	0.01054	0.02621	0.00045	0.00842	0.00039	161.9	9.1	166.8	2.8
B176–G+B–19	11.9	230	363	0.63	0.18235	0.01710	0.02722	0.00065	0.00888	0.00048	170.1	14.7	173.1	4.1

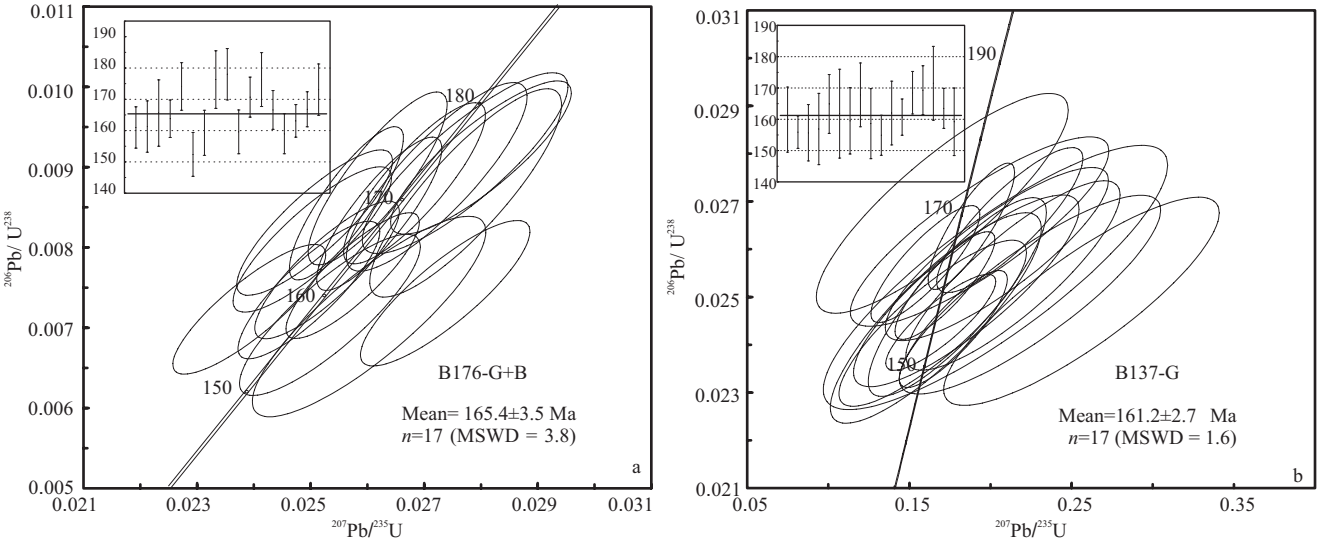

Fig. 9. U–Pb concordant diagrams and the weighted average $^{206}Pb/^{238}U$ ages of the zircons collected from the Lagkor Tso olivine diabase sample B176–G+B (a) and quartz dioritesample B137–G (b).

ratios range between 0.36and 0.87 and are mostly concentrated between 0.5 and 0.8(Table 2), indicating magmatic origin. Total 19 spots were analyzed in the sample, among which 17 spots yield a weighted mean $^{206}Pb/^{238}U$ age of 165.4±3.5Ma (MSWD = 3.8) (Fig. 9a). Considerably low age-dating figure at Point B176–G+B–11 and B176–G+B–16, in order to avoid excessive errors, dates of the two points were excluded from weighted average age calculation.

The zircon grains from the sample B137-G are mostly euhedral, transparent, colorless and up to ca. 200 μm long. The grains display oscillatory zoning with no relict core and narrow zone under CL images(Fig. 8b). Their Th/U ratios range between 0.25and 0.82 and are mostly concentrated between 0.3 and 0.5 (Table 2), indicating magmatic origin. Total 19 spots were analyzed in the sample, among which 17 spots yield a weighted mean $^{206}Pb/^{238}U$ age of 161.2±2.7 Ma (MSWD =1.6) (Fig. 9b).

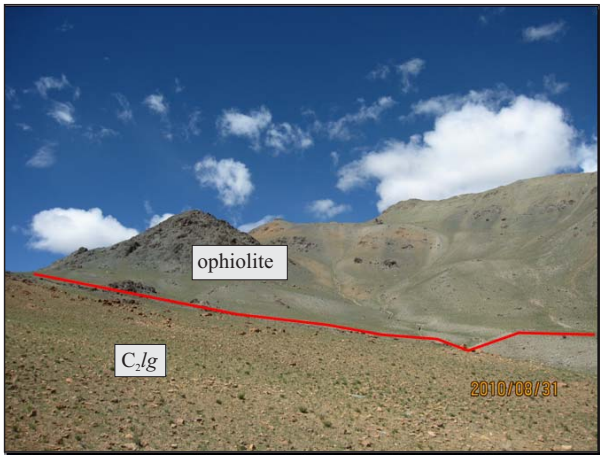

Fig. 10. Lagkor Tso ophiolite contacts with Lagar Formation by faults.

Due to larger error in age dating at Point B137-G-13, and considerably high age-dating figure at Point B137-G-18, in order to avoid excessive errors, dates of the two points were excluded from weighted average age calculation.

4.5 $^{40}Ar/^{39}Ar$ dating

The Lagkor Tso ophiolite is in fault contact with conglomeratic slate of Lagar Formation to the north. At the bottom of this ophiolite, different ophiolite unit contacts with the Carboniferous strata via a thrust fault zone with a width of 10–20 m (Fig. 10), in which the main sedimentary rock has undergone intense metamorphic deformation. We collected a sample of amphibolite plagioclase (XLG-10) for $^{40}Ar/^{39}Ar$ dating from this fault zone. In this, second generation hornblende developed along the fractures and along the plagioclase cleavage with secondary acicular hornblende. Based on the mineral composition and structure, we consider the protolith to have been a gabbro.

The $^{40}Ar/^{39}Ar$ dating results are listed in Table 4 with errors of 2σ. $^{40}Ar/^{39}Ar$ laser stepwise heating of the amphibole XLG-10 yielded a flat age spectrum, with a plateau age of 137.90 ± 6.39Ma (Fig.11; 99.62% of the total ^{39}Ar released for eight steps from 2 to 9, MSWD = 1.11). An isochron constrained by the plateau data corresponds to an age of 150.42 ± 14.27 Ma (Fig.11), which is in agreement with the plateau age.

5 Discussions

5.1 Tectonic setting discrimination

In the tectonic setting discrimination diagram plotted using Zr, Nb and Y contents (Fig. 12a), the pillow basalts

Table 4 Ar–Ar stepwise heating results

step	Laser Power(%)	^{36}Ar(a)	^{37}Ar(ca)	^{38}Ar(cl)	^{39}Ar(k)	^{40}Ar(r)	Age±2σ (Ma)	^{40}Ar(r) (%)	^{39}Ar(k) (%)
1	4	0.00000	0.00000	0.00000	0.00000	0.000054	122.2±468.0	4.65	0.39
2	5.0	0.000008	0.000000	0.000000	0.000113	0.000827	120.35±39.06	25.08	6.07
3	6.0	0.000010	0.000050	0.000001	0.000587	0.005181	144.23±8.44	63.81	31.49
4	7.0	0.000013	0.000009	0.000001	0.000482	0.003809	129.59±11.93	49.43	25.87
5	8.0	0.000003	0.000048	0.000000	0.000128	0.000935	120.12±31.62	51.05	6.87
6	10.0	0.000007	0.000015	0.000000	0.000213	0.001754	134.85±20.72	47.66	11.43
7	12.0	0.000003	0.000065	0.000000	0.000213	0.001799	138.12±19.20	63.98	11.44
8	15.0	0.000001	0.000000	0.000000	0.000076	0.000743	159.11±43.27	65.39	4.08
9	20.0	0.000002	0.000036	0.000000	0.000044	0.000299	111.76±77.50	32.43	2.37

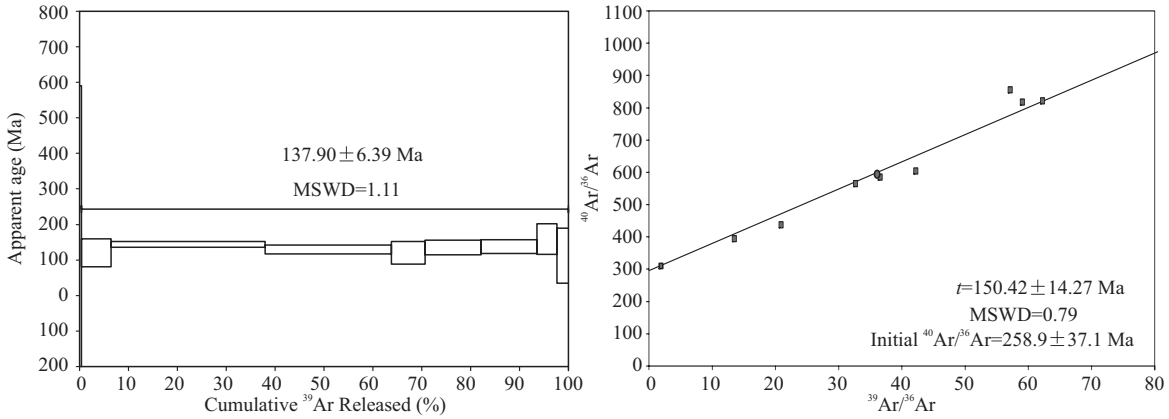

Fig. 11. Age spectrum (left)and normal isochron (right) of ^{40}Ar/^{39}Ar dating of amphibole. All of the errors are shown in 2σ.

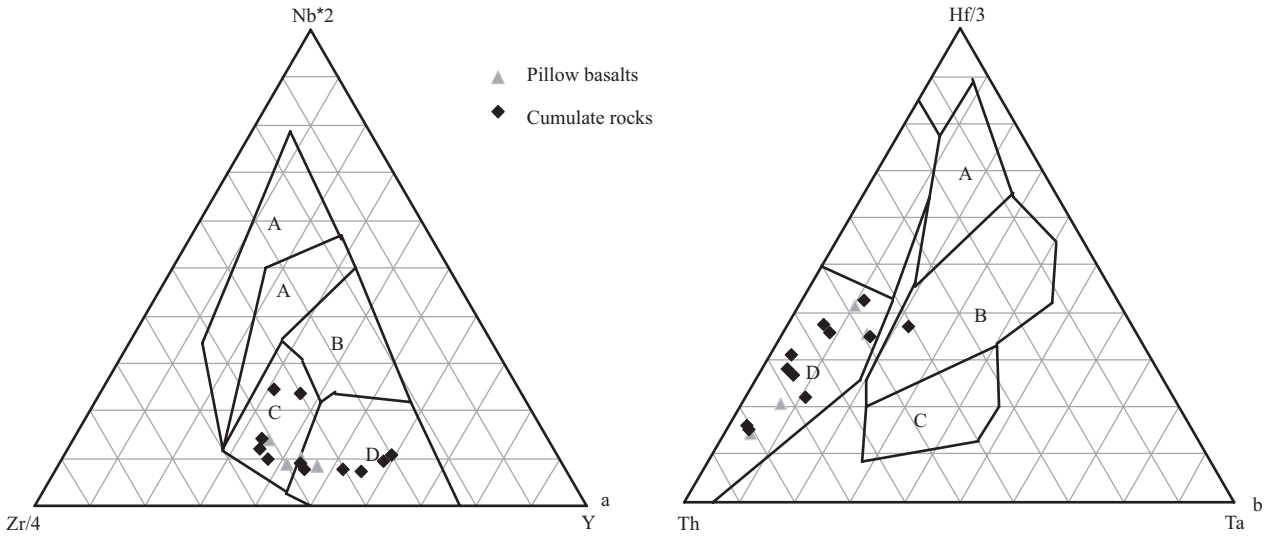

Fig.12. Tectonic discrimination diagrams for the volcanic rocks in the Lagkor Tso region.
In left diagram, AI, within–plate alkali basalts; AII, within–plate alkali basalts and within–plate tholeiites; B, E–type MORB; C,within–plate tholeiites and volcanic–arc basalts; D, N–type MORB and volcanic–arc basalts. The plotting coordinates for the boundary lines given by Meschede (1986).
In right diagram, A, N–type MORB; B, E–type MORB and within–plate tholeiites; C, within–plate alkali basalts; D, volcanic–arc basalts (Island–arc tholeiites plot in field D where Hf/Th>3.0 and calc–alkaline basalts where Hf/Th <3.0). The plotting coordinates for the boundary lines given by Wood (1980).

and the cumulate rocks plot in or near the regions of within-plate tholeiites and volcanic-arc basalts, N-type MORB and volcanic-arc basalts. In the triangle discrimination diagram able to distinguish N-MORB from E-MORB and island-arc tholeiites from calc-alkaline basalts plotted by Th, Hf/3 and Ta (Fig.12b), the pillow basalts together with the cumulate rocks plot in the area of island-arc calc-alkaline basalts. However, the Lagkor Tso ophiolite displays typical characteristics of Island-arc basalt and E-MORB characteristic chondrite-normalized Rare Earth Element (REE) patterns. Therefore, while the Lagkor Tso ophiolite was formed in subduction zone (SSZ) environment, this setting allows for potential the superposition with the development of ocean island hotspots.

In terms of geological structure, the Lagkor Tso

ophiolite borders the Langshan limestone to the north, and is covered locally by molasse sediments of Cretaceous Jingzhushan Formation (K_2j) with angular unconformity. Zenong Group volcanic rocks, mainly comprising andesitic basalt, andesite, dacite, rhyolite and volcaniclastic rocks, are distributed discontinuously upon the basement at Lagkor Tso, and were formed in an island arc setting associated with the southward subduction and consumption of the Bangonghu-Nujiang Ocean (Pan et al., 2003, 2006; Zhu et al., 2006). Thus, the island arc volcanic rocks in of the Zenong Group formed at the southern margin of the Bangonghu-Nujiang Ocean during its early southward subduction, suggesting that the Lagkor Tso ophiolite was trapped above a subduction zone (SSZ). However, the ophiolite differs from the typical N-MORB that formed in a back-arc basin. Considering this, in addition to the existence of the Zenong Group volcanic rocks and Dong Tso oceanic crust, we suggest that the formation of the Lagkor Tso ophiolite formed in island arc or inter arc environment of an SSZ is a more reasonable conclusion.

5.2 Formation and emplacement time of the Lagkor Tso ophiolite

In addition to providing clues to the tectonic environment of its formation, the ophiolite also preserves geochronological information that can constrain the evolution of the oceanic basin. At present, the accepted views on the age of Lagkor Tso oceanic basin are as follows (Table 5). (1) Geochronology is mainly judged from radiolarian fossils preserved in cherts; these fossils have generally been used to estimate the uppermost limit of the ophiolite formation. (2) Only a small number of inaccurate isotopic dates have been presented. There are few studies into emplacement time, and these mostly rely on dates from the overlying rocks of the Jingzhushan Group. Zhang *et al.* (2007) presented $^{40}Ar/^{39}Ar$ dates of 151–153 Ma for three samples of mica grains from syn-tectonic schists, which likely represent the timing of development of the Lagkor Tso oceanic basin. Thus, datings carried out by different authors and dating by different methods have resulted in considerable discrepancies in formation and emplacement time.

In this paper, more creditable and reasonable LA-ICP-MS zircon U-Pb ages of 165.4 ± 3.5 Ma (MSWD = 3.8) and 161.2 ± 2.7 Ma (MSWD =1.6) were obtained from the olivine diabase and quartz diorite respectively, which are interpreted to contain the spreading of the Lagkor Tso oceanic basin such that, at 166Ma, there should be a mature oceanic basin developed in the study area. We also obtained a $^{40}Ar/^{39}Ar$ plateau age of 137.90 ± 6.39 Ma (2σ) for the amphibolite. In the evolution of the ophiolites, the most intense and extensive deformation event should be the dynamothermal metamorphism that occurs during their emplacement. Therefore, we suggest that the $^{40}Ar/^{39}Ar$ ages represent the emplacement time of the ophiolite. The dating results show that the ocean basin split in 166 Ma at the earliest and began its subduction around 152 Ma (Zhang et al., 2007). However, this 152 Ma date could represent a node time in the process of subduction, rather than complete closure of the ocean. Recent studies have shown that ocean subduction and emplacement can be a long-term multiphase process, or that the slab can also expand whilst being subducted. It is reasonable for our $^{40}Ar/^{39}Ar$ age to be considered as the emplacement time of the ophiolite, as the 134.07 ± 0.77 Ma (MSWD = 1.8) age of Zhabuye-north body from the south side of the Lagkor Tso ophiolite is consistent with the zircon U-Pb age presented by Du *et al.* (2011) and the age of the overlying rocks of the Early Cretaceous Jingzhushan Group.

5.3 Evolution model of the Lagkor Tso ophiolite

Based on the characteristics of geological structure, geochronology and tectonic setting, we divide the evolution of the Lagkor Tso ophiolite into five major stages, all occurring within the tectonic setting of the Bangonghu-Nujiang suture zone (Fig.13).

5.3.1 Bangonghu-Nujiang rift and initial ocean stage (Permian)

During the Early Permian (around 280 Ma), under the action of mantle plume magmatism, the Bangonghu-Nujiang zone entered into the rift-development stage followed by a change in the continental features of the northern Gondwana rim. The Lhasa terrane and southern Qiangtang terrane hosted similar sedimentary formations

Table 5 Chronology of the Lagkor Tso ophiolite

Researchers	Ages	Time	Methods	Experimental subjects
Xizang Bureau of Geology and Mineral Resources, 1986	155.3±2.6 Ma	Late Jurassic	SHRIMP, paleontology	Radiolarian fossils and Zircon from plagiogranite
Xizang Bureau of Geology and Mineral Resources, 1986	124 Ma	Early Cretaceous	K–Ar	Basalt whole rock
Geology investigation institute of sichuan province, 2006	124.63±0.6 Ma	Early Cretaceous	$^{40}Ar/^{39}Ar$	Gabbro whole rock
Zhang et al., 2007	166.6±2.5 Ma	Middle Jurassic	SHRIMP	Zircon from plagiogranite
Zhang et al., 2007	151–153 Ma	Late Jurassic	$^{40}Ar/^{39}Ar$	mica grains from syn–tectonic schists

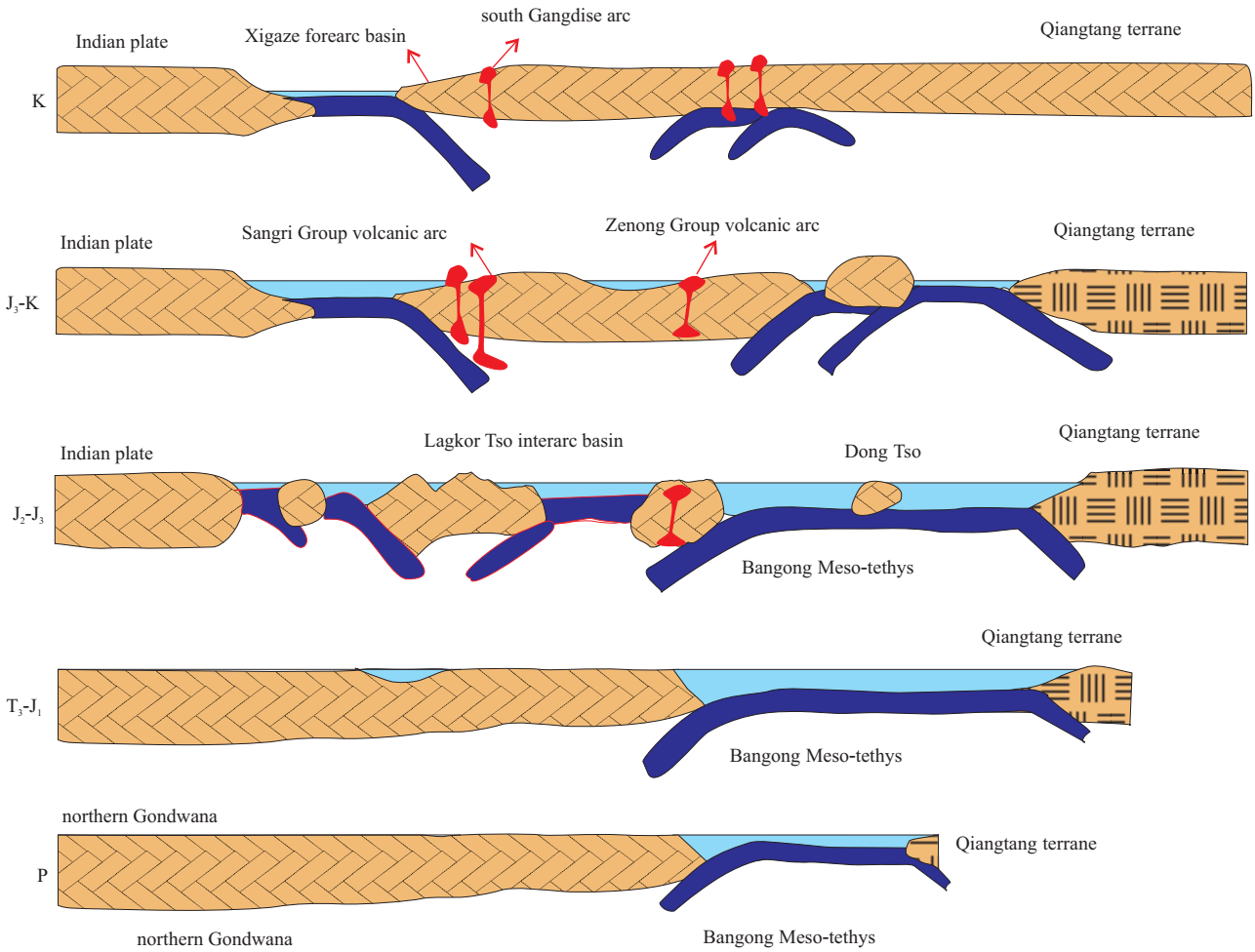

Fig.13. Simplified geodynamic model for the evolution of the Bangong Meso–tethys during the late Paleozoic – Mesozoic.

and mixed cold-warm faunae. Mantle plume magmatism seems to be the driving force behind the dissociation of the northern rim of the Gondwana Land during the Permian, also leading to glacial melting and rapid biological proliferation as a result of the environmental change that occurred between the Carboniferous and the Early Permian (Zhang et al., 2007). In the western-central segment of the Bangonghu-Nujiang zone no Permian MOR-type ophiolites like those developed in the Dingqing-Nujiang zone have been found. In addition, the terranes on both sides of the Banginghu-Nujiang zone have similar sedimentary fossil features.

5.3.2 Bangonghu-Nujiang Ocean Basin rift expansion stage (Late Triassic to Early Jurassic)

The West Bangonghu-Nujiang oceanic crust is represented by ophiolites and Early Jurassic Mugagangri Group flysch sedimentation within the suture zone. The ocean basin was situated at the northern edge of the Gangdise landmass. During the Triassic period the entire region of Tibet was under the influence of a tensional stress field. The crust of the Gangdise-Nyainqentanglha region began to separate from the continent beginning with the northern side, forming an initial marginal sea basin on the Bangonghu-Nujiang continental margin. On the northern side of the study region ophiolite samples have been collected from Shemagou at Dong Tso and Qushenla, and zircon SHRIMP dating of the gabbro from the ophiolite samples has been conducted, providing formation ages for the Dong Tso ophiolites of 221.6 ± 2.1 Ma and 190.8 ± 2.7 Ma (Zeng Qinggao, 2011). These ages may represent the time at which the ocean basin initially formed and expanded. In the Jiangcuo and Darucuo regions of Bange County there are Upper Triassic Quehala Group flysch sedimentary rocks, in disconformable contact with the Lower Permian series and the lower part of this unit is intercalated with andesite and rhyolite. It is therefore considered that both types of rocks represent early-stage rift-type volcanics. During the Early Jurassic the rift expanded further, and the marginal sea basin on the Bangonghu-Nujiang continental margin developed into a deep-ocean basin, forming oceanic crust in a manner similar to that seen in normal oceanic ridge expansion. At the same time, local upwelling of enriched-mantle

occurred, leading to the formation of hot spots within the ocean crust, and superimposing the expansion ridge and the enriched mantle beneath the oceanic crust on both sides, with the deposition of Early Jurassic Mugagangri Group abyssal flysch.

5.3.3 Main development of the Bangonghu-Nujiang Oceanic Crust: development of the Lagkor Tso and Asuo Ocean Basins (Middle and Late Jurassic)

During the Middle to Late Jurassic the West Bangonghu-Nujiang ocean basin continued expanding. Further melting of the mantle beneath the spreading ridge led to its further expansion. At the same time, the Bangonghu-Nujiang Ocean was subducting southwards. Dehydration of the subducting oceanic crust materials caused partial melting of the continental mantle wedge, forming the second-order expanding center of the obduction dish. This led to inter-arc expansion, followed by the formation of inter-arc and back-arc basins with island arc features; these basins are represented by ophiolites around the Shiquanhe-Lagkor Tso-Yongzhu region. The environment at this time may be considered similar to that of the current Western Pacific where a large number of island arc-ocean basin systems are developed. Within the Bangonghu-Nujiang basin, the Middle and Late Cretaceous Lagongtang Formation and the Early Cretaceous Langshan Formation were deposited, while at the same time, the Lagkor Tso ophiolite was formed bearing the characteristics of an SSZ. Meanwhile in the Shenzha-Namtso-Nagquri region on the southern side of the Bangonghu-Nujiang ocean basin, an EW-extending calc-alkalic island-arc zone of volcanic rocks was formed, comprising the Lagongtang Formation and the Daxiong Group volcanic rocks. In addition, an intrusion of granodiorite has also been observed in this region.

5.3.4 Transiation of the Bangonghu-Nujiang Ocean Basin from expansion to convergence: Initial emplacement of the Lagkor Tso Ophiolite (Late Jurassic-Early Cretaceous)

At the beginning of the Late Jurassic the subduction of the Bangonghu-Nujiang Ocean led to the formation of Late Jurassic-Early Cretaceous island-arc calc alkalic magmas represented by the Qusongbo Group and Zenong Group volcanic rocks. At this time, as a result of this its increased distance from the spreading center, the tectonic setting of the Bangonghu-Nujiang suture zone changed from expansion to convergence, leading to the simultaneous subduction of the Bangonghu-Nujiang Ocean in both the southern and the northern direction. During this period, the ocean basin represented by the Lagkor Tso ophiolite also began to subduct and the Lagkor Tso ophiolite began its initial emplacement. Accompanying this subduction, the Zenong Group volcanic arc was developed in the southern part of Lagkor Tso. The emplacement age for the Lagkor Tso ophiolite of 152.61±1.8 Ma obtained by our predecessors (Zhang et al., 2007) can be explained as a record of emplacement events at this time. These events were accompanied by a series of magmatic activities, leading to the development of the Lagkor Tso tectonic magmatic zone to the south of the ocean basin represented by the Lagkor Tso ophiolite.

5.3.5 Remnant ocean basin convergence, ophiolite emplacement and continent-continent collision-orogenesis: Secondary emplacement of the Lagkor Tso Ophiolite (Early Cretaceous onwards-)

During the late Early Cretaceous, the West Bangonghu-Nujiang remnant ocean basin experienced further convergence followed by continent-continent collision of the Gangdise and the South Qiangtang landmasses. With the closure of the Bannu ocean basin the ophiolites experienced a secondary tectonic emplacement. The emplacement age of the Lagkor Tso ophiolite found in the present study is 137.90 ± 6.39 Ma, while the Rejiao ophiolite in the Bangonghu region was found to have a collision-uplift emplacement age of 126.30 ± 20.45 Ma (Xia et al., 2009, unpublished data); these dates represent the emplacement events occurring in this stage. During the late Early Cretaceous the continental-facies molasse formation is widely in unconformity with the overlying Early Cretaceous strata.

After the late Early Cretaceous, the remnant ocean basin was fully subducted and passed into an intracontinental orogenesis stage. This orogenesis is marked by a series of tectonic deformation assemblages, with well-developed thrust faults, ductile shear zones and superposed folds and shear folds. Under the influence of the closure and collision of the ocean basin, the Lagkor Tso ophiolite began to emplace into its current location at this time.

6 Conclusions

The ancient Lagkor Tso oceanic basin split during the Middle Jurassic (161.2 ± 2.7 Ma–165.4 ± 3.5 Ma), and experienced a secondary tectonic emplacement in the Early Cretaceous (137.90 ± 6.39 Ma). We consider that the Lagkor Tso ophiolite developed and was emplaced in an independent suture zone. The Bangonghu-Nujiang Ocean subducted southwards, and the dehydration of subducting oceanic crust materials caused partial melting of the continental mantle wedge, forming the second-ordered expansion center of the obduction dish. This led to inter-

arc expansion, followed by the formation of inter-arc and back-arc basins with island arc features, represented by the ophiolites around the Shiquanhe-Lagkor Tso-Yongzhu region. The prevailing tectonic environment at this time is thought to be similar to that of the current Western Pacific, where a large number of island arc-ocean basin systems are developed.

Acknowledgements

We are grateful for the constructive reviews by three anonymous referees. We appreciate Qi Liang, Tu Xianglin and Qiu Huaning for their assistance during experiments and Zhou Guoqing, Zhang Yuquan, Zhong Lifeng, Huang Wei, and Zeng Qinggao for their helpful discussion. This work was supported by the National Nature Science Foundation of China (grant No.41372208) and China Geological Survey (grant No.1212011221105 and 1212011121259).

Manuscript received Nov. 1, 2014
accepted Feb. 20, 2015
edited by Hao Qingqing

References

Allègre, C.J., Courtillot, V., Tapponnier, P., Hirn, A., Mattauer,M., Coulon, C., Jaeger, J.J., Achache, J., Schaerer, U.,Marcoux, J., Burg, J.P., Girardeau, J., Armijo, R., Gariepy,C., Goepel, C., Li Tindong, Xiao Xuchang, Chang Chenfa, Li Guangqin, Lin Baoyu, Teng Jiwen, Wang Naiwen, Chen Guoming, Han Tonglin,Wang Xibin, Deng Wanming, Sheng Huaibin, Cao Yougong, Zhou Ji,Qiu Hongrong, Bao Peisheng, Wang Songchan, Wang Bixiang, Zhou Yaoxiu and Xu Ronghua., 1984. Structure and evolution of the Himalaya-Tibetorogenic belt. *Nature*, 307: 17–22.

Bao Peisheng, Xiao Xuchang, Su Li and Wang Jun, 2007. Petrological,geochemical and chronological constraints for the tectonic setting of the Dongco ophiolite in Tibet. *Science in China Series D: Earth Sciences,* 50: 660–671.

Chang Chenfa, 1988. The geological evolution of Tibet, *in* Report of the 1985 Royal Society-Academia Sinica Geotraverse of the Qinghai-Xizang Plateau. *Royal Society*, 1–413.

Coleman,R.G., 1977. What is an Ophiolite? *in* Ophiolites, Springer Berlin Heidelberg, 1–7.

Condie, K.C., 1989. Geochemical changes in baslts and andesites across the Archean-Proterozoic boundary: Identification and significance. *Lithos*, 23: 1–18.

Cox, K.G., Bell, J.D., and Pankhurst, R.J., 1979. *The interpretation of igneous rocks*. London: Georege, Allen and Unwin.

Dietz, R.S. and Holden, J.C., 1970. Reconstruction of Pangaea: breakup and dispersion of continents, Permian to present.*Journal of Geophysical Research*, 75: 4939–4956.

Geology investigation institute of sichuan province, 2006. 1:25 00000 regional geological survey report in Oma. (in Chinese)

Girardeau, J., Marcoux, J., Allegre, C.J., Bassoullet, J.P., Tang Youking, Xiao Xuchang, Zao Yougong and Wang Xibin, 1984. Tectonic environment and geodynamic significance of the Neo-Cimmerian Donqiao Ophiolite, Bangong-Nujiang suture zone, Tibet. *Nature*, 307: 27–31.

Girardeau, J., Marcoux, J., Fourcade, E., Bassoulet, J.P., and Tang Youking, 1985. Xainxa ultramafic rocks, central Tibet,China: Tectonic environment and geodynamic significance. *Geology*, 13: 330–333.

Gueddari, K., Piboule, M. and Amosee, J. 1996. Differentiation of platinum-group element (PGE) and of gold during partial melting of peridotites in the lherzolitic massifs of the Betico-Rifean range (Ronda and Beni Bousera). *Chemical Geology*, 134: 181–197.

Kapp, P., Murphy, M.A., Yin An, Harrison, T.M., Ding Lin and Guo Jinghu, 2003. Mesozoic and Cenozoic tectonic evolution of the Shiquanhe area of western Tibet. *Tectonics*, 22: 1029–1053.

Lai Shaocong and Liu Chiyang, 2003. Geochemistry and genesis of the island-arc Ophiolites in Anduo area,Tibetan plateau.*Acta Petrologica Sinica*, 19: 675–682 (in Chinese with English abstract).

Li Jianfeng, Xia Bin, Xia Lianze, Xu Lifeng, Liu Weiliang, Cai Zhourong, Yang Zhiqing, 2013. Geochronology of the Dong Tso Ophiolite and the Tectonic Environment. Acta Geologica Sinica (English Edition), 87 (6): 1604–1616.

Li Jingao and Qu De, 1993. CuoQin-Namucuo suture zone geological characteristics and prospecting significance. *Geology of Tibet*, 10: 38–44 (in Chinese with English abstract).

Liu Wei liang, Xia Bin, Zhong Yun, Cai Jianxin, Li Jianfeng, Liu Hongfei, Cai Zhourong and Sun Zhilei, 2014. Age and composition of the Rebang Co and Julu ophiolites, central Tibet: implications for the evolution of the Bangong Meso-Tethys. *International Geology Review*, 56: 430–447.

Liu Yongsheng, Gao Shan, Hu Zhaochu, Gao Changgui, Zong Keqing and Wang Dongbing, 2010. Continental and oceanic crust recycling-induced melt-peridotite interactions in the Trans-North China Orogen: U-Pb dating,Hf isotopes and trace elements in zircons frommantle xenoliths. *Journal of Petrology*, 51: 537–571.

Liu Yongsheng, Hu Zhaochu, Gao Shan, Günther, D., Xu Jun, Gao Changgui and Chen Haihong, 2008. In situ analysis of major and trace elements of anhydrousminerals by LA-ICP-MS without applying an internal standard.*Chemical Geology*, 257: 34–43.

Lorand, J.P., 1989. Abundance and distribution of Cu-Fe-Ni sulfides, sulfur, copper and platinum-group elements in orogenic type spinel lherzolites massifs of Ariege (Northeastern Pyrenees, France).*Earth and Planetary Science Letters*, 93: 50–64.

Ludwing, K.R., 2003. *Isoplot: A geochronological toolkit for Microsoft Excel.* Special Publication:Berkeley, CA,Berkeley Geochronology Center, 1–70.

Melcher, F., Grum, W. and Thalhammer, T.V., 1999. The giant chromite deposits at Kemporsai, Urals: Constraints from trace element(PGE, REE) and isotope data. *Mineralium Deposita*, 34: 250–272.

Melson, W.G., Vallier, T.L., Wright, T.L., Byerly, G., and Nelen, J., 1976. Chemical diversity of abyssal volcanic glass erupted along Pacific, Atlantic, and Ocean sea-floor spreading centers,

in the Geophysics of the Pacific Ocean Basin and Its Margin. American Geophysics Union, Washington, D.C., 351–367.

Meschede, M., 1986. A method of discriminating between different types of mid-ocean ridge basalts and continental tholeiites with the Nb-Zr-Y diagram. *Chemical Geololgy*, 56: 207–218.

Norrish, K., and Hutton, J.T., 1969, An accurate X-ray spectrographic method for the analysis of a wide range of geological samples.*Geochimica et Cosmochimica Acta*, 33:431–453.

Oshin, J.O., and Crocket, J.H., 1982. Noble metals in Thetford Mines ophiolites, Quebec, Canada, Part I: Distribution of gold, iridium,platinum, and palladium in the ultramafic and gabbroic rocks. *Economic geology and the bulletin of the society of economic geologists*, 77: 1556–1570.

Pan Guitang, Chen Zhiliang, Li Xingzhen, Yang Yangji, Xu Xiaosong, Xu Qiang, Jiang, Xinsheng, Wu Yinglin, Luo Jianning, Zhu Tongxing and Peng Yongmin, 1997. *Geological-tectonic evolution in the eastern Tethys*. Beijing: Geological Publishing House, 1–218(in Chinese).

Pan Guitang, Ding Jun and Yao Dongsheng, 2004. Geological Map of Qinghai-Xizang (Tibet) Plateau and Adjacent Areas (with a Guidebook)(1: 1, 500, 000) . Chengdu: Chengdu Cartographic Publishing House (in Chinese).

Pan Guitang, Li Xingzhen, Wang Liquan, Ding Jun and Chen Zhiliang, 2002. Preliminary division of tectonic units of the Qinghai-Tibet Plateau and its adjacent regions. *Geological Bulletin of China*, 21: 701–707.(in Chinese with English abstract).

Pan Guitang, Mo Xuanxue, Hou Zengqian, Zhu Dicheng, Wang Liquan, Li Guangming, Zhao Zhidang, Geng Quanru and Liao Zhongli, 2006. Spatial-temporal framework of the Gangdese Orogenic Belt and its evolution.*Acta petrologica sinica*, 22:521–523(in Chinese with English abstract).

Pan Yusheng, 1996. *Geological evolution of the Karakorum and Kunlun Moutains*. Beijing:Seismological Press, 1–288.

Pearce, J.A., 1983. Role of the sub-continental lithosphere in magma genesis at active continental margins, *in* Hawkesworth, C.J. and Norry, M.J. eds. Continental basalts and mantle xenoliths, Nantwich, Cheshire: Shiva Publications, 230–249.

Pearce, J.A., and Deng, W., 1988. The ophiolites of the Tibet geotraverse, Lhasa to Golmud (1985) and Lhasa to Kathmandu (1986). *Philosophical Transactions of the Royal Society A*, 327: 215–238.

Pearce, J.A., 1982. Trace element characteristics of lavas from destructive plate boundaries, *in* Andesites: orogenic andesites and related rocks. Ed. Thrope, R.S., New Youk: John Wiley and Sons, 525–548.

Pearce, J.A., Lippard, S.J., and Roberts, S., 1984. Characteristics and tectonic significance of supra-subduction zone ophiolites, *in* Kokelaar B P and Howells M F. eds.Marginal Basin Geology, J.Geological Society of London Special Publication, 16.London: Blaekwell Scientific Publications, 77–94.

Prichard, H.M., and Lord, R.A., 1990. Platinum and palladium in the Troodos ophiolite complex, Cyprus. *Canadian Mineralogist*, 28: 607–617.

Qi Liang, Gregoire, D.C., Zhou Meifu and Malpas, J., 2003. Determination of Pt, Pd, Ru and Ir in geological samples by ID-ICP-MS using sodium peroxide fusion and Teco-precipitation. *Geochemical Journal*, 37: 557–565.

Qi Liang, Hu Jing and Gregoire, D.C., 2000. Determination of trace elements in granites by inductively coupled plasma mass spectrometry. *Talanta* , 51:507–513.

Qiu Huaning and Jiang Yingde, 2007. Sphalerite $^{40}Ar/^{39}Ar$ progressive crushing and stepwise heating techniques. *Earth and Planetary Science Letters*, 256:224–232.

Qiu Huaning, 1996. $^{40}Ar/^{39}Ar$ dating of the quartz samples from two mineral deposits in western Yunnan (SW China) by crushing in vacuum. *Chemical Geology*, 127: 211–222.

Qiu Huaning, Wijbrans, J., Brouwer, F., Yun Jianbing, Zhao Linghao and Xu Yigang, 2010. Amphibolite facies retrograde metamorphism of the Zhujiachong eclogite, SE Dabieshan: $^{40}Ar/^{39}Ar$ age constraints from argon extraction using UV - laser microprobe, in vacuo crushing and stepwise heating.*Journal of Metamorphic Geology*, 28:477–487.

Robertson, A.H., 2002. Overview of the genesis and emplacement of Mesozoic ophiolites in the Eastern Mediterranean Tethyan region. *Lithos*, 65: 1–67.

Sun, S.S., and McDonough, W.F., 1989, Chemical and isotopic systematics of oceanic basalts: Implications for mantle composition and processes, *in* Saunders, A.D. and Norry, M.J.,eds., Magmatism in the ocean basins: London, Geological Society Special Publications, 313–345.

Tibet Bureau of Geology and Minerals Resources, 1987. 1:10 00000 regional geological survey report in Gerze. (in Chinese).

Tibet Bureau of Geology and Minerals Resources,1993. The field Geological Records of Tibet,Beijing:Geological Publishing House,264–477 (in Chinese).

Wang Baodi, Xu Jifeng, Zeng Qinggao, Kang Zhiqiang, Chen Jianlin and Dong Yanhui, 2007. Geochemistry and genesis of Lhaguo Tso ophiolite in south of Gerze area-Center Tibet. *Acta Petrological Sinica*, 23:1521–1530 (in Chinese with English abstract).

Wang Songshan, 1983. Age determinations of $^{40}Ar/^{40}K$, $^{40}Ar/^{39}Ar$ and radiogenic ^{40}Ar released characteristics on K/Ar geostandards of China. *Scientia Geologica Scinica*, 4: 315–323 (in Chinese).

Wang Weiliang, Aitchison, J.C., Lo Chinghua and Zeng Qinggao, 2008.Geochemistry and geo-chronology of the amphibolite blocks in ophiolitic mélanges along Bangong-Nujiang suture, central Tibet. *Journal of Asian Earth Sciences*, 33, :122–138.

Wood, D.A., 1980. The application of a Th-Hf-Ta diagram to problems of tectonomagmatic classification and to establishing the nature of crustal contamination of basaltic lavas of the British Tertiary volcanic province. *Earth Planet Science Letters*, 50: 11–30.

Wu Zhenhan, Hu Daogong, Ye Peisheng and Wu Zhonghai, 2013. Early Cenozoic Tectonics of the Tibetan Plateau. *Acta Geologica Sinica (English edition)*, 87(2), 289–303.

Xia Bin, Wang Guoqing and Zhong Futai, 1989. *Map of ophiolites and tectono-stratigraphic terranes in Himalaya and its adjacent areas and instruction*. Lanzhou: Gansu Science and Technology Publishing House, 4–26 (in Chinese with English abstract).

Xiao Xuchang and Li Tingdong, 2000. *The tectonic evolution and uplift mechanism of the Qinghai-Tibet Plateau.* Guangzhou: Guangdong Science and Technology Press, 83–122: 137–190 (in Chinese with English abstract).

Xiao Xuchang and Wang Fangguo, 1984. An introduction to the ophiolite of China. *Acta Geoscientica Sinica*, 9: 19–30(in

Chinese with English abstract).

Ye Peisheng, Wu Zhenhan, Hu Daogong, Jiang Wan, Liu Qisheng and Yang Xinde, 2004. Geochemical characteristics and tectonic setting of ophiolite of Dongqiao, Tibet. *Geoscience*, 18:309–315 (in Chinese with English abstract).

Zeng Qinggao, 2011. *Geochemistry and Tectonic Setting of the Typical Ophiolite in Rutong and Gerze*. Guangzhou Institute of Geochemistry, Chinese Academy of Sciences (Ph.D thesis) (in Chinese with English abstract).

Zhang Kaijun, Zhang Yuxiu, Li Bing and Zhong Lifeng, 2007a. Nd isotopes of siliciclastic rocks from Tibet: Constraints on the pre-Cenozoic tectonic evolution. *Earth and Planetary Science Letters*, 256: 604–616.

Zhang Kaijun, Zhang Yuxiu, Tang Xianchun and Xia Bin, 2012. Late Mesozoic tectonic evolution and growth of the Tibetan plateau prior to the Indo-Asian collision. *Earth-Science Reviews*, 114: 236–249.

Zhang Qi and Zhou Guoqing, 2001. *Ophiolites of China*. Beijing: Science Press, 1–200 (in Chinese).

Zhang Qi, Zhou Guoqing and Wang Yan, 2003. The distribution of time and space of Chinese ophiolites, and their tectonic settings. *Acta Petrologica Sinica*, 19:1–8 (in Chinese).

Zhang Yuxiu, Zhang Kaijun, Li Bing, Wang Yang, Wei Qinguo and Tang Xianchun, 2007b. Zircon SHRIMP U-Pb geochronology and petrogenesis of the plagiogranites from the Lagkor Lake ophiolite, Gerze, Tibet, China. *Chinese Science Bulletin*, 52: 651–659.

Zhou Guoqing, 1996.A review and discuss on the concept of ophiolite. *Study on Ophiolites and Geodynamics*. Beijing: Geological Publishing House, 15–20 (in Chinese).

Zhou Meifu, Malpas, J., Robinson, P.T., and Reynolds, P.H., 1997. The dynamothermal aureole of the Donqiao ophiolite (northern Tibet). *Canadian Journal of Earth Sciences*, 34: 59–65.

Zhu Dicheng, Zhao Zhidan, Niu Yaoling, Dilek, Y., Hou Zengqian and Mo Xuanxue, 2013. The origin and pre-Cenozoic evolution of the Tibetan Plateau. *Gondwana Research*, 23: 1429–1454.

About the first author

YUAN Yajuan, female; born in 1986 in Hefei city, Anhui Province; doctor; a research assistant of School of Marine Sciences, Sun Yat–sen University. She has focused on the ophiolites and tectonic evolution of the suture zone.